OPTICAL PROPERTIES OF $Se_{100-x}Bi_x$ THIN FILMS DEPOSITED ON GLASS SUBSTRATES BY FLASH EVAPORATION METHOD

BY

MULAMA AUSTINE AMUKAYIA

A THESIS SUBMITTED IN PARTIAL FULFILMENT OF THE REQUIREMENTS FOR THE DEGREE OF MASTER OF SCIENCE IN PHYSICS

DEPARTMENT OF PHYSICS AND MATERIALS SCIENCE

MASENO UNIVERSITY

ABSTRACT

The global need for sustainable energy production is pushing scientific research towards the development of inexpensive thin film solar cells which can compete with established commercial silicon-based technologies. These solar cells must be nontoxic and readily available away from cadmium telluride and gallium doped copper indium diselenide. For example, selenium and bismuth elements are nontoxic and readily available on the market. Further, selenium-bismuth alloy system is photosensitive to electromagnetic radiation. The optical properties of this system especially the absorption coefficient and the optical band gap energy are very important in the absorption of light energy. The study investigated optical properties of flash evaporated amorphous selenium-bismuth $Se_{100-x}Bi_x$ $(x = 0, 1, 2, 3, \& 4\ at.\%)$ thin films deposited on cleaned glass substrates at temperatures of 51°C, 55°C, 59°C and evacuated to $3.0 \times 10^{-5} mbar$. The study objectives were; to investigate the effect of film thickness and the effect of substrate temperature on the optical properties of selenium-bismuth alloy thin films. Thin films of thicknesses $350 \pm 10nm$, $400 \pm 10nm$, $450 \pm 10nm$ and $500 \pm 10nm$, measured on a surface profiler were selected. Their transmittance and reflectance were measured on SolidSpec.3700 Deep Ultra Violet Spectrophotometer $(200nm - 3000nm)$. It was observed that addition of bismuth led to increase in the reflectance (R), absorption coefficient (α), refractive index (n), extinction coefficient (k), real (ε_1) and imaginary (ε_2) parts of the dielectric constant for the deposited thin films. However, the transmittance (T) and band gap energy (E_g) decreased at specific wavelengths or photon energies. At a wavelength of $750nm$ or $1.655eV$ and film thickness of $350 \pm 10nm$, the optical constants calculated were; $0.683 \leq T \leq 0.815$, $1.263eV \leq E_g \leq 1.352eV$, $7.350 \leq \varepsilon_1 \leq 9.014$, $0.167 \leq \varepsilon_2 \leq 0.651$, $2.722 \leq n \leq 2.962$, $0.028 \leq k \leq 0.093$, $0.180 \leq R \leq 0.331$, and $1.641 \times 10^4 cm^{-1} \leq \alpha \leq 2.011 \times 10^4 cm^{-1}$. The optical constants were also observed to vary with film thickness and substrate temperature. The deposited amorphous selenium-bismuth alloy thin films have improved sensitivity to sun light as can be observed from the high absorption coefficient in the order of $10^4 cm^{-1}$. The band gap energy and the absorption coefficient values exhibited by the films are good for the formation of selenium-bismuth thin film solar cells.

CHAPTER ONE

INTRODUCTION

Background

world depends on fossil fuels (85%): coal, oil, and natural gas for energy [1]. The energy nand keeps on increasing and the consumption will increase even faster with the population)wth and the development of the underdeveloped regions. Not only the world but our country :nya is in a severe crisis of electricity. There are many rural areas which are still deprived from e wonder of electricity [2]. The restricted storage of fossil fuels on the earth and environmental roblems concomitant with their usage are presently putting forward the search of alternative lean renewable energy as an imperative issue for the boom of future global economy.

Due to the geographical location of our country, we get sun throughout the year. We are in a much better location for utilizing solar energy. It can be used in areas where there is no grid connection. Over the past years, more and more but still a minority of solar power has been exploited to supply a sustainable and clean electricity based upon the well-established silicon technology, despite that the price/performance ratio remains a big challenge [3]. In the pursuit of more affordable fashions for the conversion of solar to electric power, thin film solar cell technology has received an ever-increasing amount of scientific and industrial attention in the foregone two decades, owing to its feasibility to serve as a low-cost candidate in appeasing the future planetary energy demand. At the moment, one big challenge towards its large-scale application relies on how to realize less toxic and readily available thin film materials.

allium doped copper indium diselenide (CIGS) is at the moment the industrially used thin film aterial with the highest efficiency (~15%) and can compete with multicrystalline silicon [4]. or CIGS thin film solar cells, minimizing indium usage in photovoltaic (PV) cells is one very mportant concern as it is rare and expensive. Gallium and aluminium can be used as substitutes for indium. More use of gallium introduces additional defects that to date have been detrimental for the devices. Solar cells with aluminium substituted for indium have achieved efficiencies inferior to the ones with gallium [4, 5]. Both cadmium sulphide (CdS) and cadmium telluride (CdTe) that are used to make thin film solar cells are toxic to the environment and human beings. There is need to search for alternative materials that can be used to produce thin film solar cells but friendly to the environment.

Selenium is a member of group VI of the periodic table. Elements found in this group are called chalcogens: sulphur, selenium, and tellurium [6]. Addition of other elements like germanium, antimony, lead, gallium, etc. to these chalcogen elements yields chalcogenide glasses. Chalcogenide glasses are future prospective materials which would provide less expensive technical devices in the field of optoelectronics, owing to their versatile thermo-physical, optical, mid-infrared and electrical properties [7]. Hence, the area of chalcogenide glasses or non-oxide glasses especially selenium-based chalcogenides is still growing and open for investigation.

Selenium is a semiconductor [7, 8]. It has weakly bonded electrons occupying a band of energy called the *valence band*. When energy exceeding a certain threshold, called the *band gap energy*, is applied to a valence electron, the bonds are broken and the electron is free to move around in a new energy band called the *conduction band* where it conducts electricity through the material. Thus, the free electrons in the conduction band are separated from the valence band by the band gap (measured in units of electron volts or eV). This energy needed to free the electron can be

supplied by photons, which are particles of light. Further selenium has the unusual property of conducting electricity better in the light than in the dark, and is used to make photocells and solar cells [8]. It has high absorption coefficient, is nontoxic and readily available on market. However, pure amorphous selenium is unstable and less sensitive to electromagnetic radiation in standard operational conditions because its glass transition temperature (*about* 42°C) is close to room temperature putting it in perpetual danger of crystallization [9]. In order to stabilize these glasses, it is common to add certain additives (antimony, indium, lead, bismuth etc.) which act as cross-linking agents and increase the dimensionality of structure and stability of the selenium chalcogenide glass. The glass transition temperature of stabilized selenium is about70°C [9]. Bismuth alloys well with selenium. Bismuth is nontoxic, and when it combines with selenium it creates compositional and configurational disorder in amorphous selenium glassy alloys. This improves the photosensitivity of the amorphous selenium thin films. In addition, bismuth is the only element from group V of the periodic table that produces remarkable changes in the optical properties and causes p-to-n transition in conductivity of amorphous selenium thin films [6, 10].

Various studies on amorphous selenium have been done. However, there are inadequate available studies on the optical characterization of the binary selenium (Se)-bismuth (Bi) alloy thin films. The only work done on the optical properties of amorphous Se-Bi alloy thin films is by *Majeed Khan et al.* [11]. Since then there has been a shift towards the electrical characterization of the Se-Bi alloy thin films yet the optical characterization with respect to substrate temperature and film thickness is important in many device applications like in solar cell formation. In the optical investigation on amorphous Se-Bi alloy thin films by *Majeed Khan et al.* [11] and in the optical properties of ternary tellurium-selenium-bismuth alloy thin films by *Kumar et al.* [12], the optical band gap was observed to decrease with increase in bismuth

content. All the authors did not consider studying the effect of substrate temperature and film thickness on the said films. Substrate temperature induces modification in the deposited thin films which in turn affects the energy band gap of the films. The method of deposition by both authors was thermal evaporation in which the deposited thin films must be left in the deposition chamber for twenty four hours for them to be stable and to preserve the composition in the films. In flash evaporation method the stability and composition of the deposited thin films is preserved without having to leave the films in the deposition chamber for twenty four hours [13].

To have a more sensitive thin film, we have chosen the atomic percentages of bismuth to be < 5 $atomic\ percent$ $(at.\%)$ [11-13]. Since crystallization increases as bismuth content increases, then the chosen at. % is preferred. This ensures that no crystallites are found dispersed throughout the selenium-bismuth matrix.

1.2 Statement of the problem

Apart from silicon thin film solar cell, photovoltaic (PV) technology is dominated by cadmium telluride (CdTe) and gallium doped copper indium diselenide (CIGS). However, these materials have existing drawbacks: toxicity and scarcity. This limits their commercial deployment. To produce low-cost, environment-friendly, and high efficiency PV cells, explorative research is on going to identify alternative thin film materials. Thin films of Selenium (Se)-Bismuth (Bi) alloy are potential candidates for solar cells due to their improved optical properties.

1.3 Study objectives

1.3.1 Main objective

To study the optical properties {Transmittance (T), reflectance (R), refractive index (n) extinction coefficient(k), absorption coefficient(α), optical band gap energy(E_g), e.t.c} of amorphous selenium-bismuth, $Se_{100-x}Bi_x$ $(x = 0, 1, 2, 3\ and\ 4\ at.\%)$ thin films deposited on glass substrates by flash evaporation method.

1.3.2 Specific objectives

a) To investigate the effect of film thickness on the optical properties of deposited selenium-bismuth, $Se_{100-x}Bi_x$ thin films.

b) To investigate the effect of substrate temperature on the optical properties of selenium-bismuth, $Se_{100-x}Bi_x$ thin films.

1.4 Justification

Dependence on petroleum (22%) and hydropower (49.7%) for electricity is currently at the upper limit [2]. Fossil fuels are the largest contribution to air pollution. The emissions, especially, carbon dioxide, methane, nitrogen and sulphur oxides are responsible for changes in the atmosphere that affect the global climate. The ever increasing global demand for low-carbon economy combined with the Kenya's Vision 2030, our scientists and engineers are compelled to seek for benign alternatives of traditional energy tactics. Among several renewable energy sources, solar is the most abundant, one to meet our future energy supply. One of the main goals of todays' photovoltaic research is the use of less semiconductor material by making the cells thinner [3]. Thinning not only saves material but also lowers production time and the energy

needed to produce the solar cells. All of these factors decrease the production costs. Researchers are currently working on thin film solar cells as it is cost effective. Most thin film solar cells are made of silicon as it is the best thin film solar cell material [14]. Due to increased demand for solar energy, other materials are being investigated for use in thin film solar cells. Indium in gallium doped copper indium diselenide is rare and expensive. Cadmium telluride and cadmium sulphide materials are toxic to both the environment and the human life. Hence, there is need to search for other less toxic and readily available materials. Selenium-Bismuth alloy is nontoxic and the individual elements are readily available on market. The studied optical properties of selenium-bismuth thin films are good for thin film solar cell formation.

1.5 Significance of the study

The studied Selenium-Bismuth alloy thin films can be used to produce thin film solar cells based on the calculated band gap energy (1.263-1.462eV) and the absorption coefficient ($\geq 10^4 cm^{-1}$). Thin film solar cell technology has a better possibility for power production at low cost compared to the traditional commercial silicon technology. This is mainly because these types of cells require low quantity of materials even when they have large area. Moreover, large-scale fabrication is feasible, through simple and low cost techniques. This will help increase cheap electricity use both in the rural and urban areas. As a result, Kenya will be globally competitive and have a prosperous economy with quality of life.

1.6 Limitations

The surface morphology and composition measurements in the deposited thin films were not done due to lack of SEM and EDX equipment.

1.7 Assumptions

The study assumed that with the correct procedure that was followed in the deposition of the films, more than 99% of the bulk composition was maintained in the deposited thin films as observed by *Marquez et al.* [13].

CHAPTER TWO

LITERATURE REVIEW

2.1 Introduction

A Chalcogenide glass contains one or more chalcogen elements: sulphur (S), selenium (Se) and tellurium (Te) from group 6 of the periodic table, in combination with elements from groups 4 or 5 of the periodic system of elements [15]. Examples of these glasses are: antimony selenide (SbSe), antimony telluride (SbTe), indium antimony selenide (InSbSe), among others. Chalcogenide glasses are covalently bonded with glass forming ability decreasing with increasing molar weight of constituent elements. In this case, sulphur has the most glass forming ability compared to both selenium and tellurium. These glasses possess very low phonon energies (about $0.0372eV - 0.0620eV$) due to their large, heavy atoms and the low frequency of vibration of metal-chalcogen bonds [16]. They are highly transparent from the visible to the mid- infrared wavelengths, have high refractive indices and are optically highly nonlinear. Their atomic structures are flexible and viscous. They possess band gap energy of about $2eV$ and therefore are regarded as amorphous semiconductors [17]. The band gap decreases in the sequence of sulphur, selenium and tellurium, reflecting enhanced metallic character. In addition, they are quite sensitive to the absorption of electromagnetic radiation and as a result, under illumination, they show a variety of photo-induced changes.

2.2 Review of previous work

Amorphous selenium (a-Se) being a glass exhibits some degree of structural relaxation effects. As a result, its refractive index and band gap energy change with time. The structure of selenium

films from X-Ray Diffraction (XRD) machine using $CuK_{\alpha_1}(\lambda = 1.5405\,\text{Å})$ is found to be amorphous in nature [18].

Amorphous selenium exhibits the unique property of reversible phase transformation, making it attractive in varied device applications like xerography, threshold switching and memory devices [19]. The drawback of pure amorphous selenium is the low photosensitivity and thermal instability. This problem has been overcome by alloying amorphous selenium with impurity atoms like bismuth, arsenide, lead, antimony, gallium, and tellurium. Amorphous selenium (a-Se) alloys are more useful as compared to pure a-Se because of the improved photosensitivity, crystallization temperature, and ageing effects [20].

Chalcogenide glasses exhibit p-type electrical conduction due to the pinning of the Fermi level arising from the trapping of the charge carriers at localized gap states [21]. Selenium doped with bismuth glasses at higher concentration of bismuth (more than or equal to 7 at. %) is a p-n type [22]. As a result, the bismuth doping becomes important in chalcogenide glasses compared to other group 5 elements like phosphorous, arsenide or antimony which do not alter the carrier type. Recently, considerable attention has been focussed on glasses of selenium-bismuth system as these materials have found application for their electrical, optical, dielectric and thermal properties. Work on the electrical [23, 24], dielectric [25], density of defect states [26, 27] and glass transition kinetics [28, 29] of selenium-bismuth alloy has been done. Inadequate data on the optical characterization of these films is found in the literature especially for binary selenium-bismuth thin films.

According to *Majeed Khan et al.* [11], vacuum evaporated 200nm amorphous selenium-bismuth, $a - Se_{100-x}Bi_x$ $(x = 0.0, 0.5, 2.5\ and\ 5.0\ at.\%)$ thin films obeys the indirect rule. The changes

in band gap may increase or decrease depending on the bismuth concentration. At low Bi concentration, the band gap energy decreased from 1.61eV to 1.12eV. This has been explained in terms of increase in density of defect states due to Bi-Se bond. In addition, the extinction coefficient increased with photon energy. The spectral range in this case was 540nm-900nm.

Thermally evaporated thin films of tellurium-selenium-bismuth, $Te_{15}(Se_{100-x}Bi_x)_{85}$ show a decrease in the optical band gap from $1.37eV$ to $1.21eV$ as Bi concentration increases from 0 to 5 at.% [12]. This decrease in optical band gap energy is related to a decrease in cohesive energy (CE) as less CE means lower bonding strength and hence a decrease in optical band gap [30]. The spectral range was 400nm-2300nm. The film thickness ranged between 335nm- 444nm.

Pandey et al. [31] have studied vacuum evaporated amorphous selenium-antimony, $Se_{100-x}Sb_x$ $(x = 2, 4, 6, and\ 10\ at.\%)$ thin films. They found out that optical band gap energy decreased with increase in antimony content from 1.48eV to 1.28eV. The spectral range used was 400nm-1100nm.

All the authors above did not take into consideration the modifications induced to the thin films due to substrate temperature, which leads to improved optical properties of the selenium alloy thin films. The spectral range considered by the authors also varies; 540nm-900nm [11], 400nm-1100nm [31] and 400nm-2300nm [12] without stating reasons as to why they chose those ranges. This is because chalcogenide glasses find application in the whole spectra from less than 200nm to more than 3000nm. In fact, the absorption coefficient of selenium-bismuth thin films is high within 200nm-500nm. The limitation in the choice of wavelength range (200nm-3000nm) for the current study was the equipment used and the environmental impacts as outlined in chapter three, section 3.4. Further, none of the authors considered studying the effect of film thickness on the

deposited binary and ternary amorphous selenium thin films, even though *Kumar et al.* [12] had different film thicknesses of the samples. Film thickness is crucial in the thin film applications like in xerography, thin film solar cells and memory devices. The disparity in the values of the optical band gap energy may indicate either the dependence of the optical properties to the morphology, crystallinity, and fabrication processes of the chalcogenides or inadequate data processing in some of the previously published works.

There are inconsistencies on refractive index found from the study of optical characterization of selenium-antimony, $Se_{100-x}Sb_x$ thin films. For instance, the refractive index increases as antimony concentration increases [31], decreases as antimony concentration increases [32] and it increases with increase in antimony content [33]. As a result, there is need to investigate the effect of film thickness and substrate temperature on the optical properties of binary selenium alloy thin films.

When choosing the impurity element to make an alloy with selenium, we are not only interested in the value of the electrical conductivity but also in its stability with respect to temperature cycling. The benefit of transition metal doping is the improved trapping of electrons to inhibit electron-hole recombination during irradiation. Decrease of charge carrier recombination results in enhanced photoactivity. It's within this context that bismuth was chosen to alloy with selenium and we investigate the optical properties of the deposited thin films with respect to substrate temperature and film thickness.

2.3 Band gap structure model for amorphous chalcogenide glasses

Amorphous materials do not possess long-range order or periodicity, but the local arrangement or short-range order is preserved, that is, the bond lengths and bond angles are very similar to

those in a crystal [34, 35]. Small fluctuations in these values give rise to tail states protruding into the forbidden gap which leads to localization of charge carriers with energies below a certain threshold. Chalcogenide glasses behave as semiconductors electronically. This is because they have a band gap, and are transparent to a given range of wavelength of light. The disorder of the amorphous chalcogenide glasses creates localized electronic states that extend into the forbidden gap [36]. These states have a profound effect on the electrical and optical properties of these glasses. The localized states act as traps and scattering centres for conduction band electrons and valence band holes. As a result, carrier mobility of chalcogenide glasses is low. Conduction mechanism is not well known and several models have been proposed.

In the Davis-Mott Model, conduction is temperature dependent [37]. At low temperature, conduction takes place by electrons hopping between mid-gap localized states. At high temperatures, conduction is due to electrons excited into localized states at the band edges. As the temperature increases further, electrons are directly excited to extended states. According to *Davis* and *Mott,* the tails of localized states are narrow and extend a few tenths of an electron volt into the forbidden gap. In addition, defects in the random network, such as dangling bonds and vacancies give rise to a band of compensated levels near the middle of the gap. The centre band may be split into a donor and an acceptor band pinning the Fermi level at the centre.

In the Small-Polaron Model, the presence of disorder in a non-crystalline solid tends to slow down a carrier leading to a localization of the carrier at an atomic site [38]. If the carrier stays at the site for a time sufficiently long for atomic re-arrangements to occur, atomic displacements in the immediate vicinity of the carrier may be induced, forming a Small Polaron. This model is generally accepted in oxide glasses.

Cohen-Fritzsche-Ovshinsky (CFO) Model was proposed specifically for chalcogenide glasses [39]. It postulates that tail states extend across the gap in a structureless distribution and the disorder is sufficiently great to cause the tails of the valence and conduction bands to overlap, leading to an appreciable density of states in the middle of the gap. As a result of band overlapping, a redistribution of electron occurs that forms negatively charged filled states in the conduction band tail and positively charged empty states in the valence band tail. This leads to self-compensation and pinning of the Fermi level close to the middle of the gap, a feature required in explaining the electrical properties of chalcogenide materials. However, the high transparency of the amorphous chalcogenides below a well-defined absorption edge suggests a very limited degree of tailing in chalcogenides.

Glass disorder makes it hard for one to develop a model for glass conductivity. Glass lacks translational symmetry. As a result, standard band structure calculations, which are derived for a periodic arrangement of atoms in crystalline materials, cannot be used [37-39]. A complete model for chalcogenide glasses must take into account the random disorder that leads to localized states in the band gap and at the band edges. The conduction properties of the glass depend on the nature and density of the localized and delocalized states.

2.4 General theory of thin film optics

For one to understand the optical behaviour of film systems, familiarization with the optical constituents of materials, their meaning, magnitude and how they depend on the way films are processed is important [40]. Optically, the electromagnetic (EM) radiation interacts with the electrons of the material. Therefore, optical properties of materials are interpreted from the knowledge of electronic structure and how it is affected by atomic structure, bonding, impurities

and defects. EM radiation propagates differently in materials than in the free space because of the presence of charge. As a result, there is a change in the wave velocity and intensity of the radiation described by the complex index of refraction (N);

$$N = n - ik \tag{2.1}$$

where n is the real index of refraction, and k is the index of absorption/extinction coefficient.

The spatially dependent portion of the electric field (E) of a wave propagating in the x direction is given by [40, 41];

$$E = E_o exp - \left(\frac{i2\pi Nx}{\lambda}\right) \tag{2.2a}$$

where E_o is the field amplitude and λ is the wavelength.

Substituting equation (2.1) in equation(2.2a), we obtain;

$$E = E_o exp - \left(\frac{2\pi kx}{\lambda}\right) exp - \left(\frac{i2\pi nx}{\lambda}\right) \tag{2.2b}$$

The real function from equation (2.2b) , $exp - \left(\frac{2\pi kx}{\lambda}\right)$, represents an exponential damping or attenuation of the wave due to some absorption process within the material. On the other hand, the imaginary exponential portion contains n and reflects propagation without absorption. All materials exhibit varying proportion of these two linked attributes of N. In the highly absorbing metals, for example, n is usually small compared to k. On the other hand, the dielectric films used for optical purposes are highly non absorbing and k is vanishingly small compared to n.

In the medium, the wave velocity (v) is given by;

$$v = \frac{c}{n} \tag{2.3a}$$

In free space, the index of refraction is unity and the wave velocity is the speed of light , c. Using equation (2.1) the complex refractive index is defined as;

$$v = \frac{c}{N} = \frac{c}{n - ik} \tag{2.3b}$$

The refractive index, n in equation $(2.3b)$ quantifies the phase velocity of the wave in the medium. The extinction coefficient, k, establishes the level of absorption. The larger the k value, the greater the rate at which the energy of the plane wave is converted into heat in the medium in which it is propagating. The value of k is zero if the medium is truly non absorbing such as a dielectric.

The attenuation of the intensity is defined by [41];

$$I \propto EE^* \text{ or } I \propto {E_o}^2 exp - \left(\frac{4\pi kx}{\lambda}\right) \tag{2.4a}$$

where, $\boldsymbol{E}^*$ is the complex conjugate of electric field $\boldsymbol{E}$ in equation$(2.2b)$.

The emergent intensity, I, is given by;

$$I = I_o \, exp - (\alpha x) \tag{2.4b}$$

where I_o is the intensity of the incident radiation in Watts/square centimetres (W/cm^2) and α is the absorption coefficient.

Relating equations $(2.4a)$ and equation $(2.4b)$ the absorption coefficient becomes [42];

$$\alpha = \frac{4\pi k}{\lambda} \tag{2.4c}$$

From which we obtain the extinction coefficient, k, as;

$$k = \frac{\alpha\lambda}{4\pi} \tag{2.4d}$$

The absorption coefficient, α, of a material indicates how light having a specific wavelength (or energy) can penetrate the material before being absorbed. The measured transmittance data can be used to obtain the absorption coefficient, α, as a function of the wavelength as [41];

$$T = \beta\, exp - \left(\frac{4\pi kd}{\lambda}\right) \tag{2.5a}$$

where k is the extinction coefficient, d is the film thickness, and β is a constant. The constant can be approximated to one for maximum transmission to get;

$$T = exp - \left(\frac{4\pi kd}{\lambda}\right) \tag{2.5b}$$

Substitution of equation$(2.4b)$ in equation$(2.5b)$ yields;

$$T = exp - (\alpha d) \tag{2.5c}$$

Taking natural logarithm on both sides of equation $(2.5c)$ and rearranging, we get;

$$\alpha = \frac{1}{d}\, In\frac{1}{T} \tag{2.6a}$$

The absorption coefficient, α, has units of reciprocal length, usually inverse centimetre (cm^{-1}) and is used to calculate the attenuation of a beam of light in an absorbing material.

Equation $(2.6a)$ can be written as;

$$\alpha = \frac{A}{d} \tag{2.6b}$$

where

$$A = In\frac{1}{T} \tag{2.6c}$$

is the absorbance.

The optical band gap, E_g, was evaluated from the standard expression [43];

$$\alpha h\nu = \xi\left(h\nu - E_g\right)^{\gamma} \tag{2.7}$$

where α is the absorption coefficient, ξ is a constant, $h\nu$ is the photon energy and $\gamma = \frac{1}{2}$ for a direct allowed transition, $\gamma = \frac{3}{2}$ for a direct forbidden transition, $\gamma = 2$ for an indirect allowed transition and $\gamma = 3$ for an indirect forbidden transition [12].

A fraction R of the total radiation energy incident on an object is reflected from the top surface and a fraction T is transmitted through the bottom surface. The remaining fraction is lost through electronic absorption (A) processes and by scattering (S) at surface and volume imperfections. Surface roughness, internal boundaries and density fluctuations arising from porosity, pinholes, micro-cracks, particulate incorporation, and impurities are sources of scattering. The total contribution is [40];

$$R + T + A + S = 1 \tag{2.8}$$

Figure 2.1 shows a typical case of light travelling from the thin film of refractive index n into the air of refractive index n_o

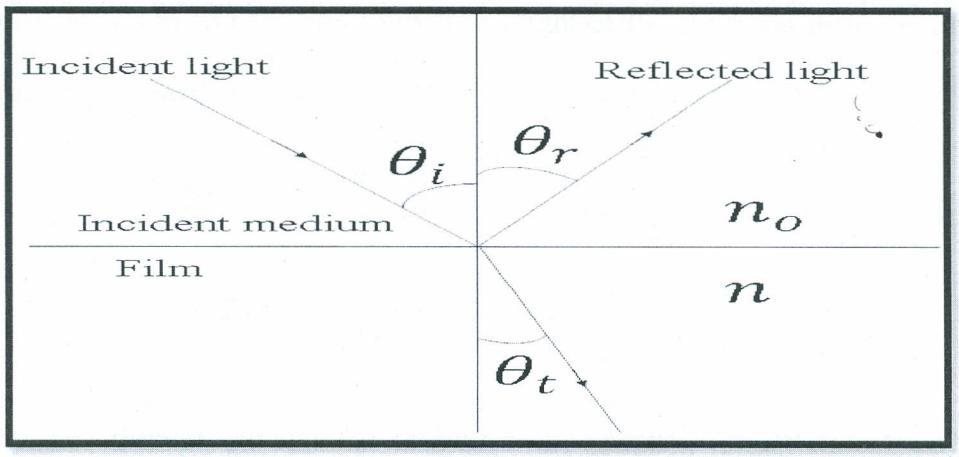

Figure 2.1: Schematic diagram of an interface between air and thin film [41].

The normal incidence amplitude reflectance at an interface between two semi-infinite, non-absorbent materials of different indices of refraction is given by the Fresnel Formula [40];

$$r_1 = \frac{n_o - n}{n_o + n} \tag{2.9a}$$

$$r_2 = \frac{n - n_o}{n + n_o} \tag{2.9b}$$

$$t_1 = \frac{2n_o}{n_o + n} \tag{2.10a}$$

$$t_2 = \frac{2n}{n + n_o} \tag{2.10b}$$

where n_o is the refractive index of air, n is the refractive index of thin film material, r is the coefficient for the amplitude of the reflected light, t is the coefficient for the amplitude of the transmitted light, r_1 and t_1 are for light travelling from the air into the thin film, r_2 and t_2 are for light travelling from the thin film into the air.

The amount of reflected (R) and transmitted (T) light at the interface in terms of the Fresnel coefficients and the refractive indices are [44] ;

$$R = r_1 r_2 = \left|\frac{n_o - n}{n_o + n}\right|^2 \tag{2.11}$$

$$T = t_1 t_2 = \frac{4 n_o n}{(n_o + n)^2} \tag{2.12}$$

If the light passes through an ambient medium with complex refractive index $n_o - ik_o$, and reflects from a thin absorbing film with thickness d and complex refractive index $n - ik$ at normal incident, we have;

$$R = \frac{(n-n_o)^2 + (k-k_o)^2}{(n+n_o)^2 + (k+k_o)^2} \tag{2.13}$$

Equation (2.13) does not depend on the film thickness.

Typically, the ambient medium does not absorb light and, in most cases it is air, where $n_o = 1$ and $k_o \cong 0$ and therefore [45];

$$R = \frac{(n-1)^2 + k^2}{(n+1)^2 + k^2} \tag{2.14}$$

For the case of a thin film on a substrate material, both the top and the bottom of the film will reflect light. The total amount of reflected light is the sum of the two individual reflections. Because of the wave nature of light, these reflections will interfere either constructively or destructively depending on their phase relationship, which is determined by the difference in the path lengths between the two reflections. The path length is in turn determined by the thickness of the film, its optical constants and the wavelength of the light wave radiation incident on the

film. For constructive interference, the reflections are in phase when the path difference is equal to an integer multiple of the wavelength of the light given by;

$$2nd = m\lambda \tag{2.15}$$

where d is the film thickness and m is an integer representing the order of reflection.

Conversely, when reflections are out of phase we get destructive interference. Here, the path difference is one half of a wavelength different from the in-phase conditions.

$$2nd = \left(m + \frac{1}{2}\right)\lambda \tag{2.16}$$

The study of optical properties of thin films, which is the main goal of this work, is based on the response of the films as it interacts with electromagnetic radiation.

2.5 Deposition methods for thin films

Deposition of thin films involves; creation of material, transport of material and deposition of material onto a substrate. Deposition techniques are classified as: Physical vapour deposition (PVD) and chemical vapour deposition (CVD). Physical methods cover deposition techniques which depend on the evaporation or ejection of material from a source, whereas chemical methods depend on a specific chemical reaction [46].

The physical vapour deposition is classified into thermal evaporation, sputtering, electron beam evaporation, molecular beam epitaxy (MBE), reactive evaporation, ion plating and flash evaporation. The objective of these deposition processes is to transfer atoms from a source to substrate where film formation and growth proceed atomistically. In evaporation, atoms are

removed from the source by thermal means, whereas in sputtering they are dislodged from target surface through impact of gaseous ions. The molecular beam epitaxy produces epitaxial films by condensation atoms from Knudsen source under ultra high vacuum. If the evaporated material is transported through a reactive gas, the deposition technique is called reactive evaporation. Ion plating refers to a process in which the substrate and the film are exposed to a flux of high energy ions during deposition. Chemical vapour deposition is the process in which a volatile chemical compound of a material reacts before being deposited onto a substrate, with other gases or condensation of compound from the gas phase onto substrate where reaction occurs to produce a solid deposit. The various chemical reactions are thermal decomposition, hydrogen reduction, nitridation, disproportionation, chemical transport reactions and combination of one or more of these reactions [40, 46]. Each of the above methods has its own advantages and disadvantages. We shall restrict to the method that will be used in this study which is flash evaporation.

Flash evaporation method is used when we have to deposit a multicomponent material that cannot be heated to the evaporation point together like selenium ($melting\ point$: 217°C) and bismuth ($melting\ point$: 271°C) in this study [47]. This technique uses the principle of thermal-resistance heating to evaporate metals. Like filament evaporation, flash evaporation offers radiation-free coatings. The technique does offer some benefits beyond filament evaporation: Contamination-free coatings, speed or good throughput of wafers, and the ability to coat materials or layers that are composite in nature. In addition, the method is cost effective and convenient for deposition of compounds. Flash evaporation is accomplished by passing a continuous supply of the material to be evaporated using an electromagnetically vibrating feeder over heated molybdenum or tungsten. On heating the material in vacuum, sublimation takes

place and the atoms are transported and get deposited onto cleaned glass substrates held at suitable distance at desired temperatures [48, 49].

2.6 Thin film applications

Thin film solar cells: Silicon solar cell technology is the most used in the formation of thin film solar cells. Despite continued incremental improvements, silicon-wafer cells have a built-in disadvantage of fundamentally high material cost and poor capital efficiency. Since silicon does not absorb light very strongly, silicon wafer cells have to be very thick. However, wafers or bulk samples are fragile and therefore their intricate handling complicates processing all the way up to the panel product. Polycrystalline thin film solar cells based on copper indium diselenide ($CuInSe_2$) and its alloys and cadmium telluride (CdTe) appear to be the most promising candidates for large scale application of photovoltaic energy conversion because they have shown laboratory efficiencies in excess of 15% [5, 48]. Heterojunction devices with n-type cadmium sulfide (CdS) films show very low minority carrier recombination at the absorber grain boundaries and at the metallurgical interface which results in high quantum efficiencies. Open circuit voltages of these devices are relatively low owing to the recombination in the space charge region in the absorber. Further improvement in efficiency can be achieved by reducing this recombination current, especially in devices based on $CuInSe_2$ and its alloys. Low-cost manufacturing of modules requires better resolution of a number of other technical issues. For modules based on $CuInSe_2$ and its alloys, the role of sodium and higher deposition rates on device performance need to be better understood. In addition, replacing the chemical bath deposition method for CdS film deposition with an equally effective, but more environmentally acceptable process is needed. For modules based on CdTe, more fundamental understanding of the effect of chloride/oxygen treatment and the development of more reproducible and

manufacturable CdTe contacting schemes are necessary. Therefore, there is need to investigate other thin film materials for use in solar cell formation like selenium-bismuth alloy thin films.

Thin films for micro-electro-mechanical systems (MEMS): Shape memory alloys (SMAs) possess an array of desirable properties; high power to weight ratio, thus the ability to recover large transformation stress and strain upon heating and cooling, pseudoelasticity (or superelasticity), high damping capacity, good chemical resistance and biocompatibility. This attracted much attention to the research of SMAs as smart (or intelligent) and functional materials [49, 50]. More recently, thin film SMA has been recognized as a promising and high performance material in the field of micro-electro-mechanical system (MEMS) applications, since it can be patterned with standard lithography techniques and fabricated in batch process. Thin film SMA has only a small amount of thermal mass to heat or cool, thus the cycle (response) time can be reduced substantially and the speed of operation may be increased significantly. The work output per volume of thin film SMA exceeds that of other micro-actuation mechanisms. The phase transformation in SMA thin film is accompanied by significant changes in the mechanical, physical, chemical, electrical and optical properties, such as yield stress, elastic modulus, hardness, damping, shape recovery, electrical resistivity, thermal conductivity, thermal expansion coefficient, surface roughness, vapour permeability and dielectric constant, etc. These changes can be fully made use of the design and fabrication of microsensors and microactuators. However, due to the lack of full understanding of the thin film SMAs together with the difficulty in controlling of the deposition parameters, they have not received as much attention in the MEMS technology as other microactuator technologies [51].

In the field of nanotechnology-based thin films, new approaches using nanoscale effects can be used to design, create or model nanocoating systems with significantly optimized or enhanced

properties of high interest to the food, health and biomedical industry. With the development of nanotechnology in various areas of materials science, there is potential use of novel nano-surfaces and more reliable nanomaterials by employing nanocomposite and nanostructured thin films in food packaging, security pharmaceutical labels, novel polymeric containers for food contact, medical surface instruments, bio-implants and coated nanoparticles for bionanotechnology [52]. Nanostructured films and packaging materials can prevent the invasion of pathogens and other microorganisms and ensure food safety. Nanosensors embedded in food packages allow the determination of food quality or nutrient content. By adding certain nanoparticles into packaging material and bottles, food packages can be made more light- and fire-resistant, with stronger mechanical and thermal performance and controlled gas absorption.

CHAPTER THREE

EXPERIMENTAL METHODS

3.1 Introduction

Methods and procedures for deposition and optical characterization of Selenium-Bismuth alloy: $Se_{100-x}Bi_x$ $(x = 0, 1, 2, 3\ and\ 4\ at.\%)$ thin films are outlined in this chapter. The glass substrates (Corning model 7059) measuring $76.2mm \times 25.4mm \times 1.2mm$ were used. The corning glass substrate is good for optical and electrical studies in thin films. Silicon, silicon IV oxide and plastic substrates are good for deposition of organic thin films. Films deposited on mica substrates may have more structural disorder because of the rough interface of film and the substrate.

3.2 Substrate cleaning

Production of high quality amorphous thin films of Se-Bi alloy with good long-term stability against crystallization requires that the films are deposited onto a substrate with a surface that is clean from oil, dust and other contaminants. If the surface of the substrate is contaminated with foreign substances like oil or grease, the adhesion of film will be degraded and there will be a tendency for the thin film to crack and peel. Amorphous selenium is unstable and tends to crystallize quickly in the presence of contaminants. Humidity and oil from human fingertips usually accelerates the crystallization process. The substrate preparation procedure used was as follows:

A mixture of deionised water, liquid detergent and sodium hydroxide in the ratio of 3:2:1 in a wash bottle was shaken to form foam. The foam was applied to a cotton swap which was used to

scrub both sides of the glass slides. Using a lens cleaning tissue folded severally and held at an angle of 45^{o} to the cleaning table, the glass slides were drag wiped to remove the foam. A new lens cleaning tissue, wet at one edge side with ethanol was used to wipe the glass slide. Using another new set of lens cleaning tissue, wet at one side with acetone, the glass slides were drag wiped. Powersonic 405 Ultrasonic cleaner with three quarters full of deionised water was used to rinse the glass slides for 30 minutes at 45°C to ensure complete removal of dirt. The cleaned glass slides were sprayed with pressurised argon gas to remove deionised water. The glass slides were used for coating immediately after the cleaning exercise to avoid contamination with the environment. Latex gloves were worn during cleaning of the glass slides to prevent the skin oils from contaminating the slides.

3.3 Deposition of $Se_{100-x}Bi_x$ thin films on glass substrates by flash evaporation method

Bulk samples of selenium-bismuth alloy, $Se_{100-x}Bi_x (x = 0, 1, 2, 3 \; and \; 4 \; at.\%)$ were prepared by melt quenching technique. Selenium and bismuth of 99.99% purity were weighed according to their atomic percentages in powder form on the electronic balance (***LIBROR, AEG-120***). The weighed samples were sealed in quartz ampoules (length was 10cm, internal diameter was 0.8cm) evacuated to 8.0×10^{-5} mbar. Chalcogenide glasses belong to substances which have an incongruent melting point, exhibit a high partial vapour pressure during melting and the melt tend to have a high viscosity and are susceptible to oxidation and hydrolysis. Therefore, the synthesis must be carried out in sealed evacuated quartz ampoules. The sealed ampoules were kept in a programmable furnace where the temperature was raised from 26°C to 800°C gradually at a rate of 4°C per minute and maintained at this temperature for 12 hours with rocking after every 30 minutes to produce homogeneous mixture [29]. Gradual increase in

temperature helps to avoid explosion that may occur. The ampoules were quenched by removing them from the furnace (at 800°C) and dropping in ice cold water. Quenching ensures that the different atoms are randomly mixed to form continuous homogeneous non-crystalline films on cleaned substrates, the films having greater than stoichiometric proportions of the non-metal component. The glass forming region obtained by quenching in ice water is much greater than that obtained from quenching in air or slow cooling. The ampoules were broken to obtain the solid alloy that was crushed into powder for flash evaporation (Figure 3.1). The method is flexible and easy to use.

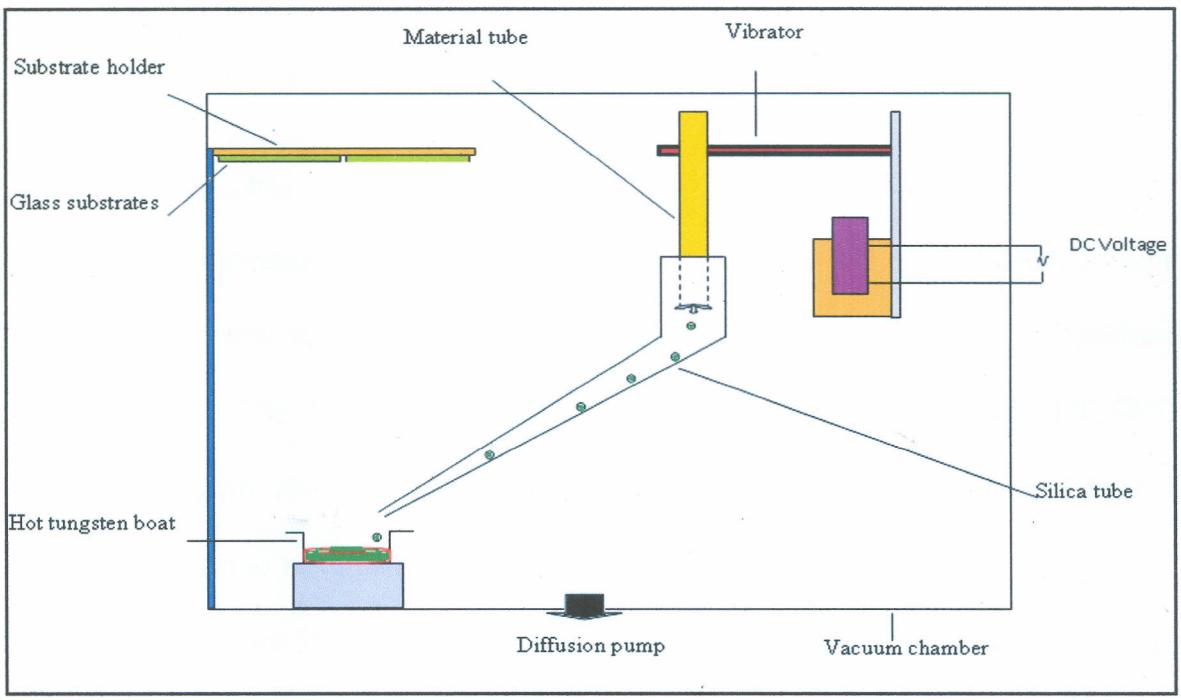

Figure 3.1: Simplified set up for flash evaporation technique.

The material powder (0.100g, 0.125g, 0.150g and 0.175g) was placed inside the material tube which was placed inside the evaporation chamber. The chamber was evacuated to $3.0 \times 10^{-5}\ mbar$ to avoid reaction between the vapour and atmosphere and to obtain good

homogeneous films (***Edwards AUTO 306 vacuum system***). The vibrator was used for dispensing powder onto the boat. A direct current voltage of $15V$ was applied across the vibrator which made it vibrate. The vibrations were transmitted to the silica tube. The powder then fell grain by grain from the vibrating material tube into the silica tube to the boat placed below, which was preheated. The deposition rate was $25Å s^{-1}$ according to the Edwards Auto 306 Vacuum System. The low deposition rate produces film composition which is very close to that of bulk starting material [13]. The substrate temperatures were; 51°C, 55°C, and 59°C. In this method, the material was created in vapour form by means of resistive heating. On heating the material in vacuum, sublimation took place and the atoms were transported and got deposited onto cleaned glass substrates held at a distance of $11cm$ from the source.

Thin films of $Se_{100-x}Bi_x$ $(x = 0, 1, 2, 3\ and\ 4\ at.\%)$ were deposited on cleaned glass substrates by flash evaporation method. At $x = 0\ at.\%$ we have Se_{100} i.e. no bismuth content. This provides the control result as selenium is the main material. The chamber pressure was $3.0\ x\ 10^{-5} mbar$. The films were deposited at substrate temperatures of 51°C, 55°C, and 59°C. This is slightly above the maximum temperature for the ratio of chains and rings in the amorphous selenium to be at balance, which is usually 50°C [9]. In fact, the results for 46°C was similar to the results for 51°C. Remarkable change was observed at 55°C. Hence, the starting substrate temperature was chosen to be 51°C. Some crystals were observed in the films deposited at a substrate temperature of 65°C, i.e. the films failed to be amorphous at this temperature. The thicknesses of the deposited films were in the range of $350 \pm 10nm, 400 \pm 10nm, 450 \pm 10nm\ and\ 500 \pm 10nm$. These films were amorphous, homogeneous and uniform. The optical properties were studied in the spectral range of $200nm\ to\ 3000nm$ on the SolidSpec.3700 Deep Ultra Violet (DUV) Spectrophotometer.

3.4 Transmittance and reflectance measurements

Both the transmittance and reflectance measurements were made using a SolidSpec.3700 Deep Ultra Violet (DUV) Spectrophotometer (***SolidSpec.3700 DUV Instructional manual***). The equipment was controlled by a personal computer (PC) interfaced to it and had a software program (Ultra Violet (UV) Probe version 2.21) for computer-controlled operation. The software controlled all SolidSpec.3700 DUV Spectrophotometer functions and included a Microsoft (MS)-Word-compatible report generator and MS-Excel compatible spread sheet for instant analysis. The software allowed all the important features to be selectable: Scanning speed, gratings, detectors, and density filters. SolidSpec.3700 DUV Spectrophotometer permits measurements that combine speed and precision far beyond those of conventional stepper-motor driven monochromator and Spectro 320 optical spectrum analyzer. It is designed to combine the advantages of the large signal dynamic range and high spectral resolution characteristics of a scanning spectrometer with the short measuring times of array detectors. The SolidSpec.3700 DUV Spectrophotometer also has an enormous spectral range. It is possible to scan from 175nm to 3300nm in the maximum configuration with 3 gratings and 3 detectors. The instrument switches automatically between each grating and detector during the scan.

In this work, Barium Sulphate ($BaSO_4$) integrating sphere (Model 198851) was used. Barium Sulphate plate was used as a reference for reflectance measurements of the $Se_{100-x}Bi_x$ film samples at normal incidence. The detectors used for this application were: Photomultiplier (PMT) (165nm-1000nm) for the ultraviolet and visible region, and indium gallium arsenide (InGaAs) (700nm-1800nm), lead sulphide (PbS) (1600nm-3300nm) detectors for the near-infrared region. The spectral range of study was 200nm - 3000nm. This is because oxygen molecules in the

atmosphere absorb UV light under 190nm. Nitrogen gas purging is required to remove the interfering oxygen molecules, a process we did not consider.

The transmittance data were used for the calculation of optical constants such as optical band gap, refractive index, extinction coefficient, and absorption coefficient according to equation (2.5a) and equation (3.3).

3.5 Thickness measurements

Film thickness was determined using a computerized KLA-Tencor Alpha-Step IQ surface profiler on which three measurements were taken at different positions of the thin film sample and the average calculated. The surface profiler characterized the surface by scanning with a diamond tipped stylus from the bare portion of the film to the coated portion. The step height was created by the movement of the stylus on the thin films. The thickness was obtained from the difference in reading between those from the bare substrate and those from film and substrate. The average film thicknesses are given in table 3.1.

Sample No.	First reading (nm)	Second reading (nm)	Third reading (nm)	Average (nm)
1	351.41	349.30	350.52	350.41
2	398.01	402.10	399.41	399.84
3	451.32	448.93	449.36	449.87
4	498.61	497.89	502.37	499.62

Table 3.1: Sample thickness measurements

The experimental error was found from equation 3.1 based on the speed or rate of the stylus and the frequency made by the stylus.

$$\delta = \frac{Speed\ of\ stylus\ (\mu ms^{-1})}{Frequency\ of\ stylus\ (s^{-1})} \tag{3.1}$$

The frequency of the stylus used was $1000s^{-1}$ and the rate at which the stylus was moving was $10\mu ms^{-1}$ (***Alpha-Step IQ User Manual, KLA-Tencor Corporation, 2004***). Hence, the error was found to be $\delta = 0.01\mu m$ *or* $10nm$. Therefore, averaged thicknesses to the nearest whole number of the deposited films were $350 \pm 10nm, 400 \pm 10nm, 450 \pm 10nm$ *and* $500 \pm 10nm$. These sequential measurements are as a result of the amount of material powder used with a difference of 0.025g. A mass of 0.025g after several trials produced about 50nm film thickness (i.e. between 48.81- 50.42nm).

3.6 X-Ray Diffraction Spectroscopy

Thin films of selenium-bismuth, $Se_{100-x}Bi_x$ $(x = 0, 1, 2, 3\ and\ 4\ at.\%)$ were characterized by the X-Ray Diffraction technique (***Phillips PW3710 XRD System***). Computer controlled Phillips PW3710 XRD and analytical X'Pert 2000 data collection software was used. This was possible because of the θ-2θ parallel beam geometry of the scan machine. The range was from 5° to 60° with detector type of continuous scan at a scan step of 0.5s and step size of 0.025°. Irradiated length was 12mm and the specimen length was 10mm with a receiving slit size of 0.1mm. The anode material was Copper (Cu) and the incident radiation source was CuK_{α_1}(λ = 1.5406Å). The intensity of the radiation was provided by the wavelength λ = 1.5406Å. The generator settings were 30mA and 40kV. The measurements were done at room temperature of 26°C.

3.7 Refractive index calculations

Refractive index (n) of a material depends upon the wavelength (λ) of light, n (λ). The method used to determine the refractive index in this study was the Swanepoel envelope method [53]. A distinct advantage of using the envelopes of the transmission spectrum rather than only the transmission spectrum is that the envelopes are slow-changing functions of wavelength whereas

the transmission spectrum varies rapidly with wavelength. Interference effects gave rise to the typical transmittance spectrum with successive maxima and minima points. The first step was to calculate the maximum and minimum transmittance envelop functions, $T_M(\lambda)$ and $T_m(\lambda)$, respectively. From these functions, n (λ) can be found [54]. The equations are only true for the section of the transmittance spectra for which the absorption coefficient is not zero ($\alpha \neq 0$)

$$n(\lambda) = [N + (N^2 - {n_s}^2)^{1/2}]^{1/2} \tag{3.2}$$

where $N = 2n_s \frac{T_M - T_m}{T_M T_m} + \frac{{n_s}^2 + 1}{2}$ (3.3)

n_s is the refractive index of the glass substrate (1.52)

CHAPTER FOUR

RESULTS AND DISCUSSIONS

4.1 Introduction

The chapter presents the research results and discussions on the flash evaporated amorphous selenium-bismuth, $Se_{100-x}Bi_x$ $(x = 0, 1, 2, 3 \; and \; 4 \; at.\%)$ thin films deposited on glass substrates at temperatures of 51°C, 55°C, and 59°C. In this work, the optical properties of deposited $Se_{100-x}Bi_x$ thin films of thicknesses $350 \pm 10nm, 400 \pm 10nm, 450 \pm 10nm \; and \; 500 \pm 10nm$ were investigated and are discussed. The optical system under investigation was amorphous, homogeneous and uniform. From the transmittance data of these thin films, refractive index (n) and extinction coefficient (k) were determined from which other optical parameters like absorption coefficient (α) and the optical band gap energy (E_g) were obtained. These are the optical parameters that define the optical characteristics of any given thin film coating material. Effect of bismuth content on the determined optical parameters has been discussed. Further, effect of film thickness and substrate temperature on the deposited thin films has been discussed. The results have been compared to already published works by other researchers.

4.2 Transmittance and reflectance of the deposited thin films

Transmittance and reflectance against wavelength (nm) for selenium-bismuth, $Se_{100-x}Bi_x$ thin films for $x = 0, 1, 2, 3, \& \; 4 \; at.\%$, at thicknesses 350nm, 400nm, 450nm and 500nm is shown in figure 4.1.

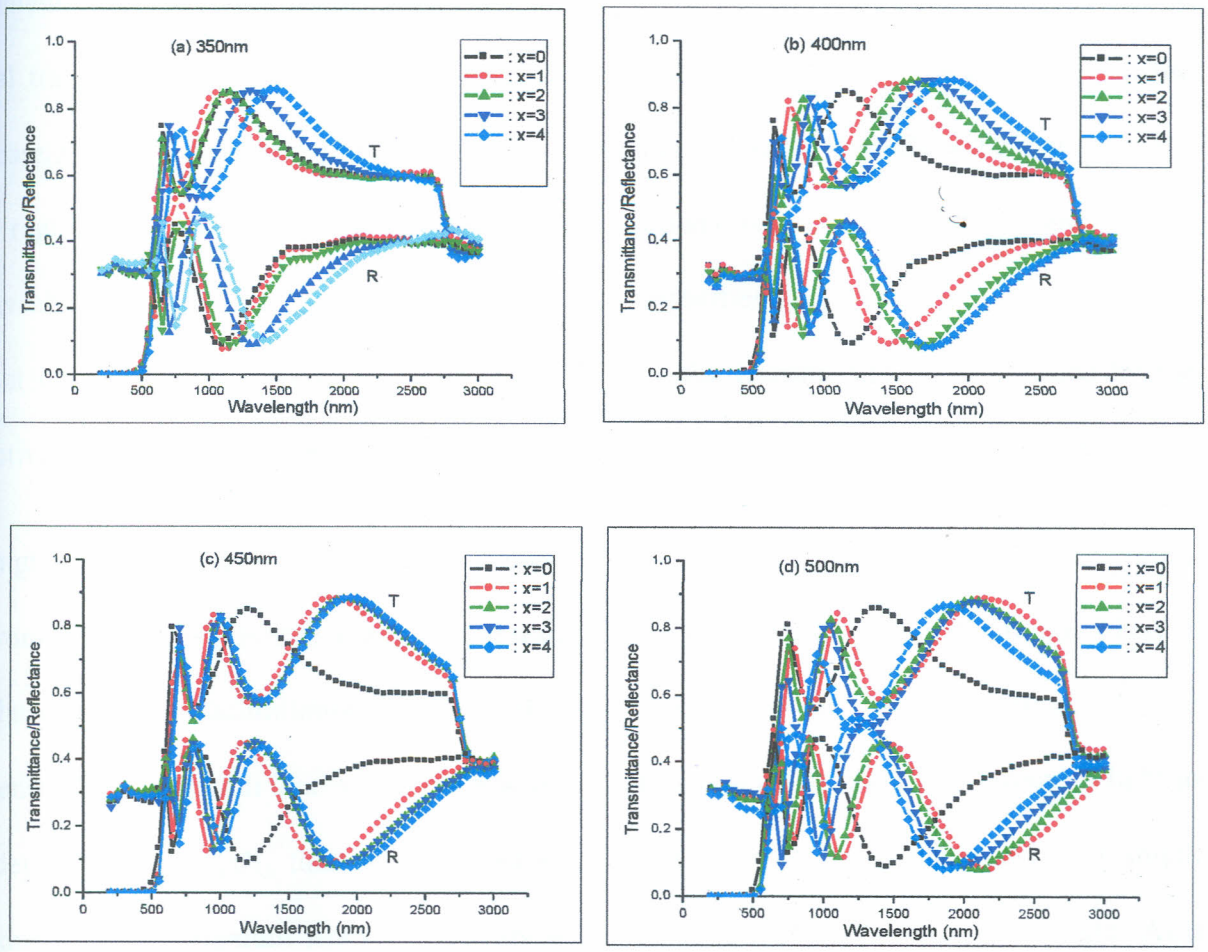

Figure 4.1: Transmittance and reflectance against wavelength (nm) for $Se_{100-x}Bi_x$ thin films at different film thicknesses; (a) 350nm, (b) 400nm, (c) 450nm and (d) 500nm

As observed from figure 4.1, there is little transmission (≤ 0.0347) at low wavelengths ($\leq 500nm$) because most of the light is absorbed. This is the region of strong absorption and has very large absorption coefficient ($7.883 \times 10^4 cm^{-1} \leq \alpha \leq 3.562 \times 10^5 cm^{-1}$). The absorption edge of the investigated thin films is in the visible spectral range, where its transmission falls to about zero values at $\lambda \approx 500nm$ [55]. The region between $500nm$ and $800nm$ has medium absorption and the transmission is ≤ 0.821. This is because of the effect of the absorption

coefficient of range $6.062 \times 10^3 cm^{-1} \leq \alpha \leq 14.108 \times 10^4 cm^{-1}$. In this region, most of the optical transitions take place between localized tail states and extended band states. In the transparent region ($\geq 900nm$), the absorption coefficient is low ($\alpha \leq 4.682 \times 10^2 cm^{-1}$). This is the region that is away from the electronic and vibrational resonances. It is the region of low energy absorption that originates from defects and impurities and in this case from bismuth content on the deposited $Se_{100-x}Bi_x$ thin films. Here, the transmission is determined by the refractive index of the film and the refractive index of the substrate through multiple reflections.

For higher wavelengths ($> 500nm$) corresponding to the low energies, there is no appropriate electronic transitions possible and therefore transmission is generally high in this range. There is a relatively sharp delimitation between the areas of high and low absorption. As the concentration of bismuth increases from $x = 0\ at.\%$ to $x = 4\ at.\%$, the transmission of light in the deposited $Se_{100-x}Bi_x$ thin films decreases. This is mainly due to the effect of bismuth introduced in the selenium films as impurity which absorbs part of the transmitted light. As a result, the absorption coefficient increases. The transmittance and reflectance versus wavelength curves (Figure 4.1) show interference fringes between the wave fronts generated at the air and substrate interface that defines the sinusoidal behaviour of the curves between $600nm$ and $2500nm$, which has also been observed by *Chauhan et al.* [56]. The interference fringes are not very strong as expected for selenium films and this could be due to effect of bismuth impurities as observed by *Wee* [57]. The interference fringes increases as the thickness of the deposited films increases from 350nm to 500nm. This reveals the smooth homogeneous film surfaces.

From figure 4.1, reflectance values increases and decreases at specific wavelengths as bismuth concentration increases from $x = 0$ to $x = 4\ at.\%$ due to effect of transmission of light in the deposited thin films.

Transmittance against bismuth concentration at different film thicknesses and wavelength $\lambda = 750nm$ is shown in figure 4.2. Increase in thickness of the deposited films led to decrease in transmittance values. This is because thick films effectively increase the absorption path length of the films. This implies that light absorption is increased. It is clear from the graph that as bismuth concentration increases from $x = 0$ to $x = 4\ at.\%$, the transmission of light decreases. This implies that the thicker the films the less transparent the films of selenium-bismuth alloy becomes. Hence, a thickness of 500nm yields less transparent films. For 350nm thin films $0.683 \leq T \leq 0.815$, $0.675 \leq T \leq 0.720$ for 400nm, $0.621 \leq T \leq 0.701$ for 450nm, and $0.582 \leq T \leq 0.675$ for 500nm thin films.

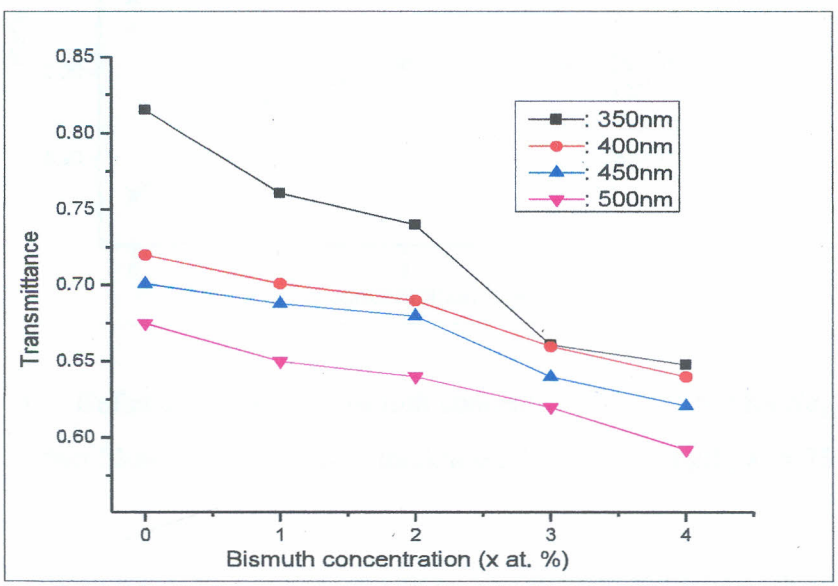

Figure 4.2: Transmittance against bismuth concentration ($x\ at.\%$) for $Se_{100-x}Bi_x$ thin films at different film thicknesses and wavelength, $\lambda = 750nm$

In figure 4.3, the graph of reflectance against bismuth concentration ($x\ at.\%$) for $Se_{100-x}Bi_x$ thin films at different film thicknesses is presented at a wavelength $\lambda = 750nm$. It is observed the figure that reflectance increases with increase in film thickness. This may be due to the decrease in transmission of light in the deposited films with increase in film thickness, an indication of less transparent films. Reflection of light in the deposited selenium-bismuth alloy thin films is low for very thin films (350nm). This correlates well with the increased transmittance for the same films as already observed from figure 4.2.

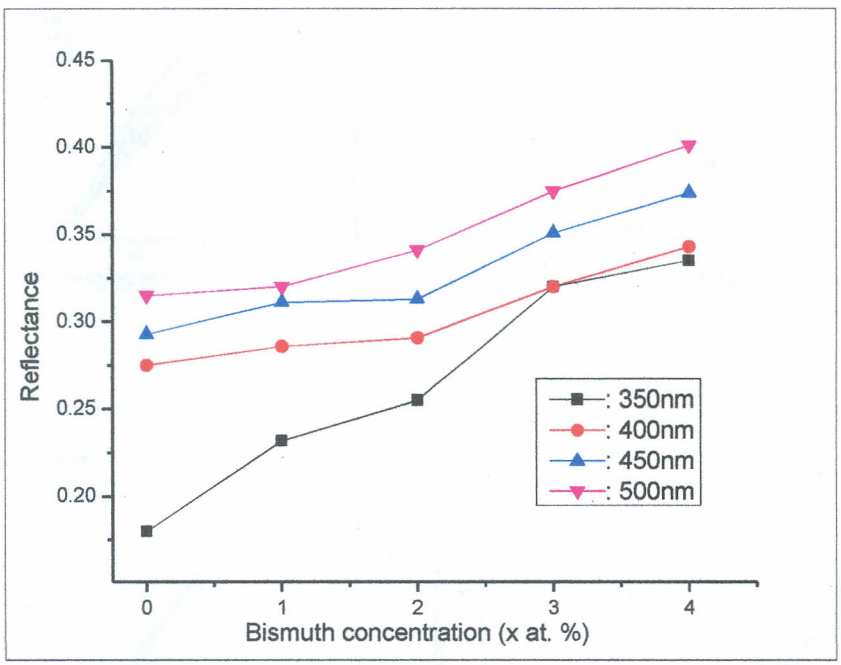

Figure 4.3: Reflectance against bismuth concentration ($x\ at.\%$) for $Se_{100-x}Bi_x$ thin films at different film thicknesses and wavelength, $\lambda = 750nm$

Reflectance against bismuth concentration as shown in figure 4.3 indicates that the reflectance increases as the bismuth concentration increases from $x = 0$ to $x = 4\ at.\%$ as a result of

decrease in transmission of light. At 350nm,$0.180 \leq R \leq 0.331$, $0.275 \leq R \leq 0.341$ for 400nm, $0.283 \leq R \leq 0.369$ for 450nm, and $0.315 \leq R \leq 0.397$ for 500nm thin films.

4.3 Absorption coefficient of the deposited thin films

Figure 4.4 shows optical absorption coefficient against photon energy (eV) at various film thicknesses.

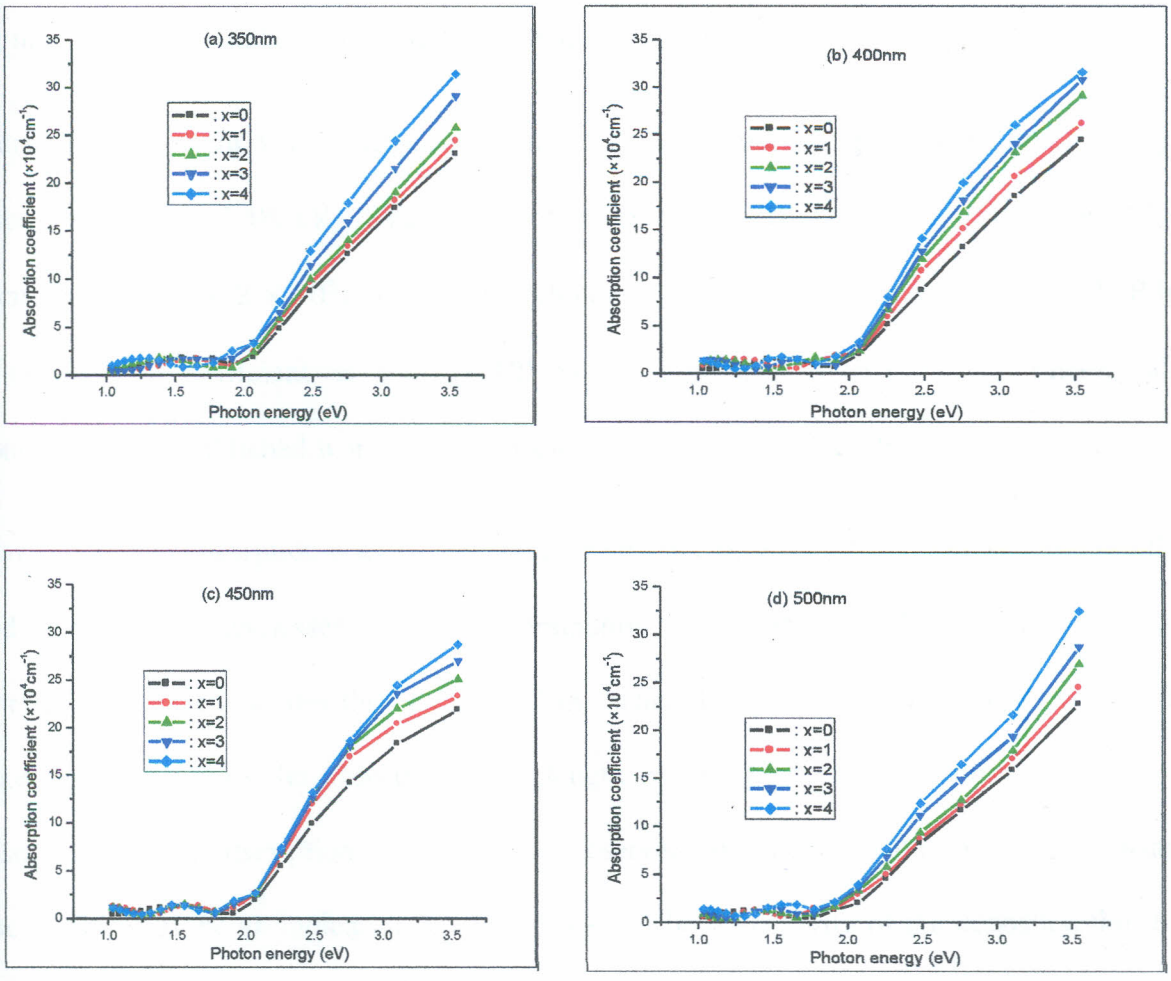

Figure 4.4: Absorption coefficient against photon energy (eV) for $Se_{100-x}Bi_x$ thin films at different film thicknesses; (a) 350nm, (b) 400nm, (c) 450nm and (d) 500nm

Absorption coefficient gradually increases with an increase in photon energy up to photon energy $2.0eV$ (350nm), $1.85eV$ (400nm), $1.80eV$ (450nm), and $1.75eV$ (500nm) after which it increases rapidly. This is an indication that thick films absorb more light photons than thin films because rapid increase in absorption coefficient is first observed in 500nm thin films compared to the other three thicknesses. This abrupt positive shift in the deposited thin films was overlooked by previous authors [11, 12, 31]. For low energies, corresponding to high wavelengths, thin film interference effects are observed. This may be due to the overlaying of light that is reflected on both sides of the deposited thin films of $Se_{100-x}Bi_x$.

Absorption coefficient values increase markedly at lower wavelengths ($\leq 500nm$) or higher photon energies ($\geq 2.483eV$). The values of absorption coefficient are in the range $7.883 \times 10^4 cm^{-1} \leq \alpha \leq 3.562 \times 10^5 cm^{-1}$. In the photon energy range of $1.552eV \leq hv \leq 2.483eV$, the absorption coefficient is $1.312 \times 10^4 cm^{-1} \leq \alpha \leq 7.577 \times 10^4 cm^{-1}$. These values surpasses already published works, hence, ideal for thin film solar cell formation.

Figure 4.5 shows absorption coefficient against bismuth concentration for $Se_{100-x}Bi_x$ thin films for different film thicknesses. A close examination reveals that the thick films have higher absorption coefficient values than the thin films. This effect may be explained by the fact that thicker films increases the absorption path length of the deposited thin films decreasing the transmittance. The absorption coefficient is observed to increase with increase in bismuth content. This may be an indication of an increase in photosensitivity of the deposited thin films with bismuth addition. This trend fits well with already published work [11]. Absorption coefficient varies with film thicknesses; $1.641 \times 10^4 cm^{-1} \leq \alpha \leq 2.011 \times 10^4 cm^{-1}$ for 350nm thin films, $1.644 \times 10^4 cm^{-1} \leq \alpha \leq 2.031 \times 10^4 cm^{-1}$ for 400nm, $1.682 \times 10^4 cm^{-1} \leq \alpha \leq 2.152 \times 10^4 cm^{-1}$ for 450nm, and $1.742 \times 10^4 cm^{-1} \leq \alpha \leq 2.324 \times 10^4 cm^{-1}$ for 500nm thin

films at wavelength of $\lambda = 750nm$. This wavelength is within the high solar optical absorption wavelength region (350nm-1000nm). Within a range of wavelength 650nm-800nm, there exists long diffusion length with low recombination velocity for excess carriers and this leads to formation of best thin film solar cells [11, 12, 33].

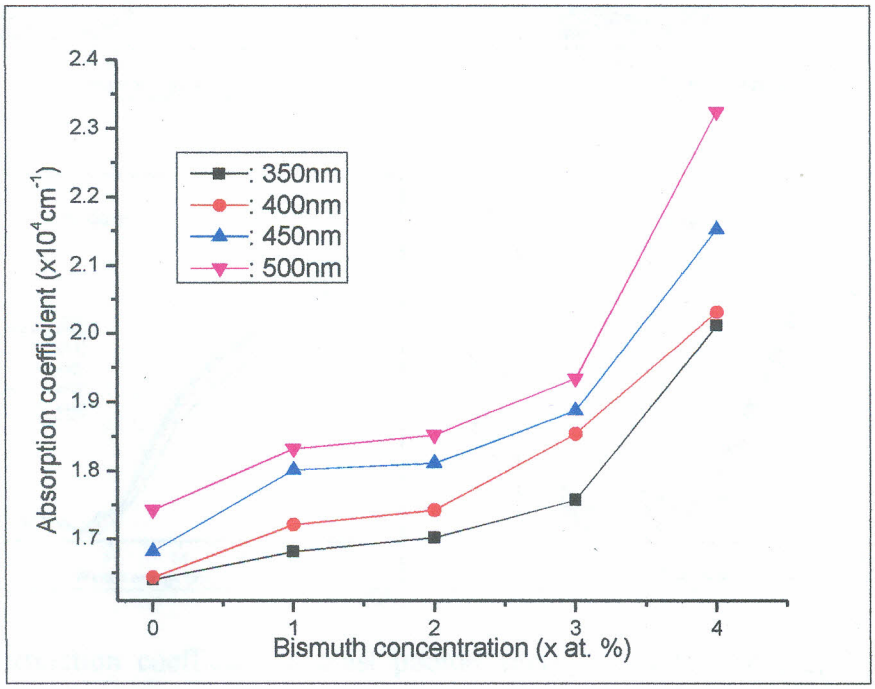

Figure 4.5: Absorption coefficient against bismuth concentration ($x\ at.\%$) for $Se_{100-x}Bi_x$ thin films at different film thicknesses and wavelength, $\lambda = 750nm$

4.4 Extinction coefficient of the deposited thin films

Figure 4.6 show plots of extinction coefficient against photon energy (eV) of the deposited thin films at different film thicknesses. Increase in extinction coefficient values with increase in bismuth concentration, results from increased absorption coefficient of the deposited thin films with bismuth concentration.

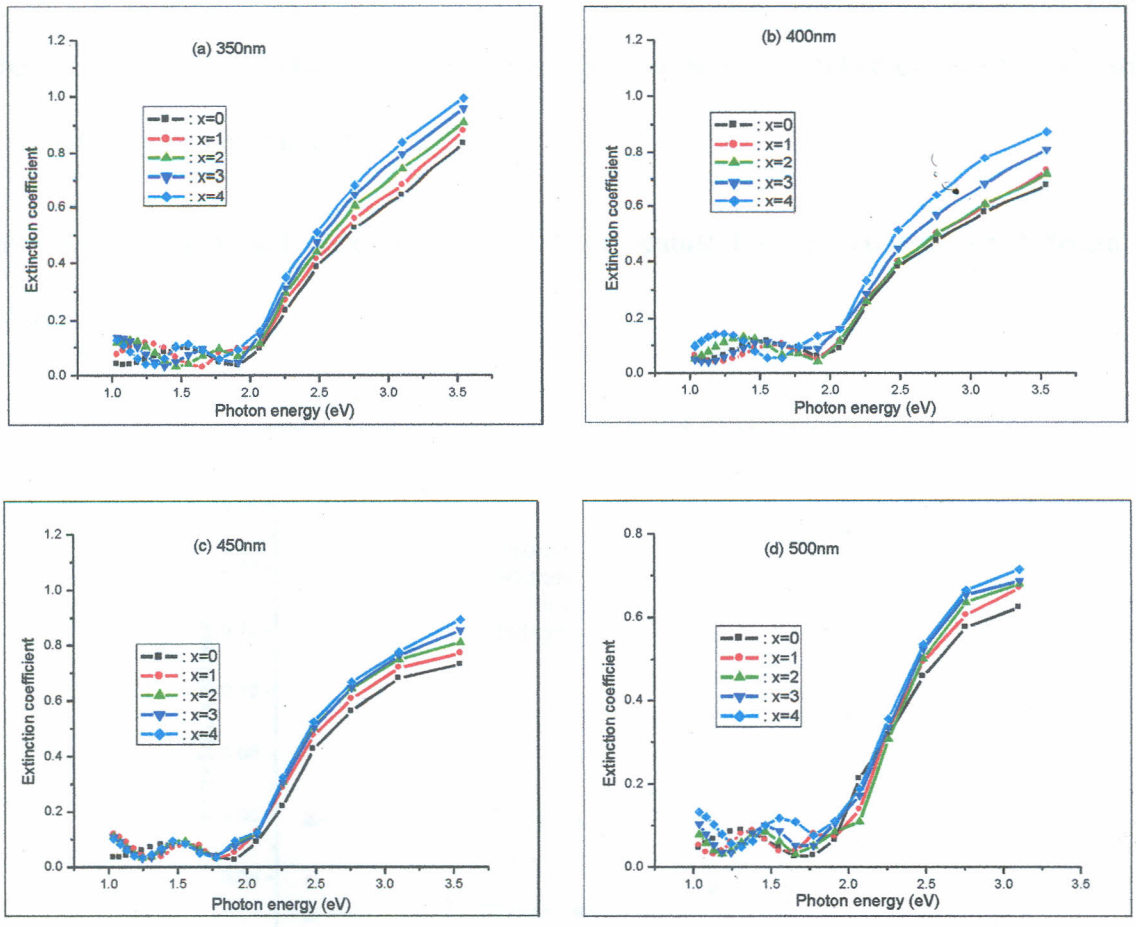

Figure 4.6: Extinction coefficient against photon energy (eV) for $Se_{100-x}Bi_x$ thin films at different film thicknesses; (a) 350nm, (b) 400nm, (c) 450nm and (d) 500nm

From the plots of extinction coefficient against photon energy (Figure 4.6), the extinction coefficient increases with increase in photon energy. This trend has been observed by *Majeed Khan et al.* [11]. The rise and fall of extinction coefficient in the forbidden gap region is directly related to the absorption of light. This behaviour increases with increase in film thickness. The shift in photon energy where extinction coefficient increases rapidly with film thickness varies. The shift for 350nm thin films starts at $1.97eV$, for 400nm thin films it is at $1.92eV$, for 450nm thin films it is at $1.90eV$, and for the 500nm thin films it is at $1.76eV$. This correlates well with

the shifts for absorption coefficient in figure 4.4 and confirms that the absorption coefficient increases with increase in film thickness. This behaviour was overlooked by the previous authors for the same system of thin films [11].

Figure 4.7 shows a plot ofextinction coefficient against bismuth content for different film thickness.

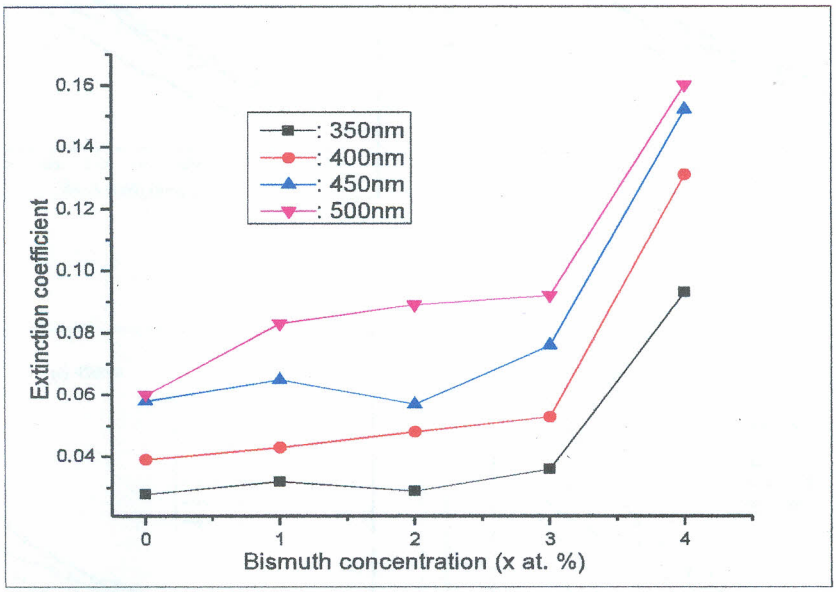

Figure 4.7: Extinction coefficient against bismuth concentration ($x\ at.\%$) for$Se_{100-x}Bi_x$ thin films at different film thicknesses and wavelength, $\lambda = 750nm$

It is observed that there is an increase in extinction coefficient with increase in the film thickness. This may be due to the increased absorption coefficient with film thickness as already shown in figure 4.4. The extinction coefficient is also observed to increase with increase in film thickness, an indication of photosensitive thin films. At a wavelength of $\lambda = 750nm$, $0.028 \leq k \leq 0.093$ for 350nm, $0.039 \leq k \leq 0.131$ for 400nm, $0.058 \leq k \leq 0.152$ for 450nm, and $0.061 \leq k \leq 0.161$ for 500nm has been observed.

4.5 Refractive index of the deposited thin films

The plots of refractive index against wavelength (nm) are shown in figure 4.8.

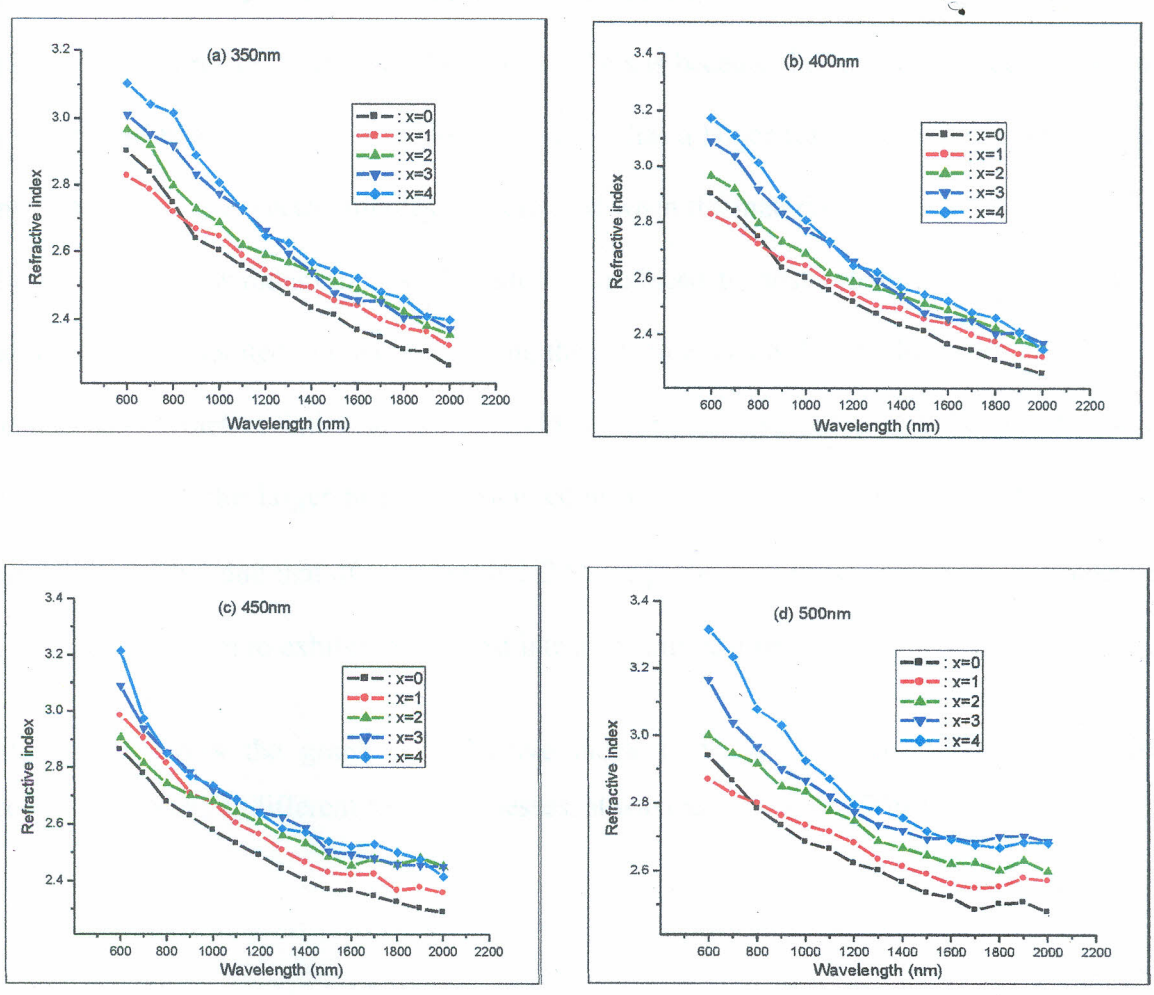

Figure 4.8: Refractive index against wavelength (nm) for $Se_{100-x}Bi_x$ thin films at different film thicknesses; (a) 350nm, (b) 400nm, (c) 450nm and (d) 500nm

Refractive index decreases with increase in the wavelength but increases with increase in bismuth concentration from $x = 0$ to $x = 4\ at.\%$. The decrease in refractive index with wavelength could be attributed to the strong effects of surface and volume imperfections in

chalcogenide glasses. It also indicates the normal dispersion in thin films. The increase of refractive index with increase in bismuth concentration agrees with the previous works [11, 33].

Increase in refractive index with increase in bismuth concentration can be explained in terms of narrowing of pores in the deposited thin films. This is because the film surface gets denser as the impurities of bismuth increase. A denser material has a larger refractive index than a less dense material since more electric dipoles are activated when the material is exposed to electric field of the incoming light radiation. As bismuth is introduced to host selenium films, bismuth atom addition is incorporated in the cross-linking the selenium chains by bonding with selenium atoms. Increase in refractive index as the bismuth content increases may also be due to increased polarizability of the larger bismuth atoms compared to selenium atoms. The atomic radius of bismuth is 1.50Å and that of selenium is 1.20Å [58]. The high polarizability of the chalcogenide glasses causes them to exhibit the highest intrinsic nonlinear response.

Figure 4.9 shows the graph of refractive index of $Se_{100-x}Bi_x$ thin films against bismuth concentration (x) at different film thicknesses, at wavelength, $\lambda = 750nm$.

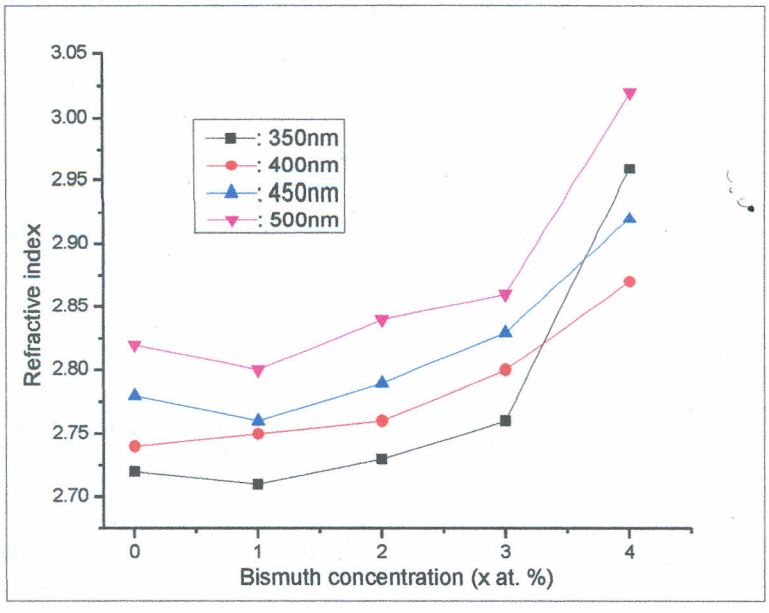

Figure 4.9: Refractive index against bismuth concentration ($x\ at.\%$) for $Se_{100-x}Bi_x$ thin films at different film thicknesses and wavelength, $\lambda = 750nm$

The refractive index of the deposited thin films generally increases with increase in film thickness. Increasing the thickness may have increased density of the deposited films leading to increased refractive index [57]. For a film thickness of 350nm, $2.722 \leq n \leq 2.962$, $2.738 \leq n \leq 2.865$ for 400nm, $2.728 \leq n \leq 2.913$ for 450nm, and $2.825 \leq n \leq 3.025$ for 500nm thin films at a wavelength, $\lambda = 750nm$. However, there is an abrupt increase in refractive index with bismuth content at $x = 3\ at.\%$. This could be the result of chemical disorder in chalcogenide glasses like selenium-bismuth under investigation. This disorder produces large charge in the local potential through the coulombian interaction because of the large ionic contribution to the bonding in chalcogenide glasses [59]. For our case of selenium-bismuth glassy alloy, this behaviour combined with the internal strain of the films due to bismuth impurities, is more pronounced in very thin films and in this case for a 350nm thickness.

4.6 Dielectric constant: real and imaginary parts

The propagation of electromagnetic waves within a medium that loses energy during its propagation like the films under investigation has complex refractive index, n^*. The response of the material to the external electric field is determined by complex dielectric response function, ε^* [40].

$$\varepsilon^* = \varepsilon_1 + i\varepsilon_2 = n^{*2} = \left(n^2 - k^2\right) + 2ink \tag{4.3}$$

where ε_1, ε_2 are the real and imaginary parts of the dielectric constant such that;

$$\varepsilon_1 = n^2 - k^2 \; ; \; \varepsilon_2 = 2nk \tag{4.4}$$

The real part of the dielectric constant shows how much it will slow down the speed of light in the material under investigation, whereas the imaginary part shows how a dielectric material absorbs energy from an electric field due to dipole motion. The knowledge of the real and the imaginary parts of the dielectric constant provides information about the loss factor which is the ratio of the imaginary part to the real part of the dielectric constant [60].

The real part of the dielectric constant against wavelength decreases with increase in wavelength as shown in figures 4.10. This behaviour is similar to that of the refractive index with wavelength. This is because the extinction coefficient on which the real part of dielectric constant depends (Equation (4.4)) is a small quantity. The real part of the dielectric constant represents the in-phase component of the dielectric response function and results in dispersion. This physically means refraction of the electromagnetic radiation as it passes through the deposited films.

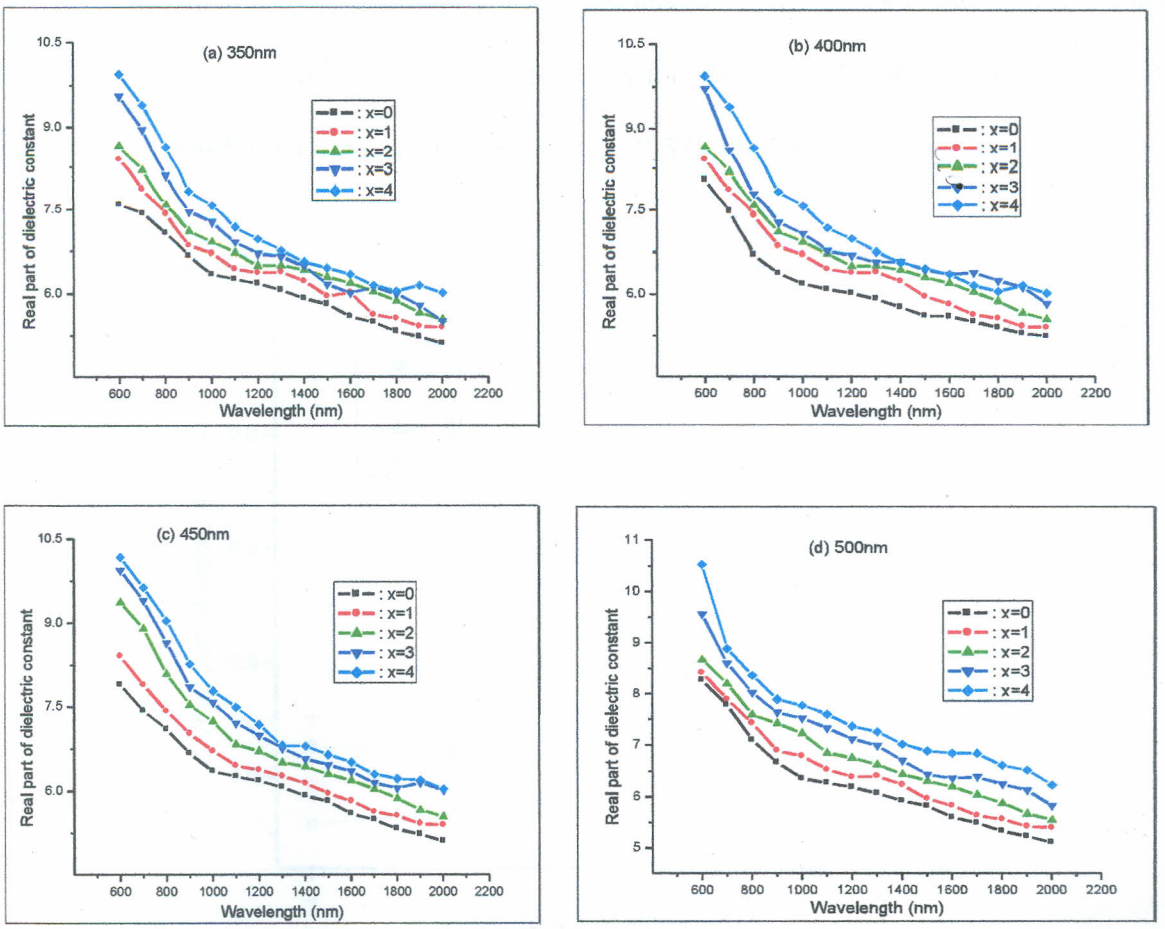

Figure 4.10: Real part of dielectric constant against wavelength (nm) for $Se_{100-x}Bi_x$ thin films at different film thicknesses; (a) 350nm, (b) 400nm, (c) 450nm and (d) 500nm

Increase in the real part of dielectric constant with bismuth concentration of the deposited thin films is observed in figure 4.11. The values of real part of the dielectric constant are greater than those for the imaginary part. This shows that the absorption coefficient of the deposited thin films is high. This trend has been observed by *Majeed Khan et al.* [11]. In addition, the real part of the dielectric constant increases with increase in film thickness mainly due to the effect of the refractive index. This is as a result of the direct proportionality between the real part of dielectric constant and the refractive index and that the extinction coefficient is a small quantity (Equation

4.4). The effect at $x = 4\ at.\%$ for the $350nm$, has already been explored under refractive index. At a wavelength, $\lambda = 750nm$, $7.350 \leq \varepsilon_1 \leq 9.014$ for 350nm, $7.501 \leq \varepsilon_1 \leq 8.375$ for 400nm, $7.611 \leq \varepsilon_1 \leq 8.945$ for 450nm, and $7.750 \leq \varepsilon_1 \leq 9.375$ for 500nm.

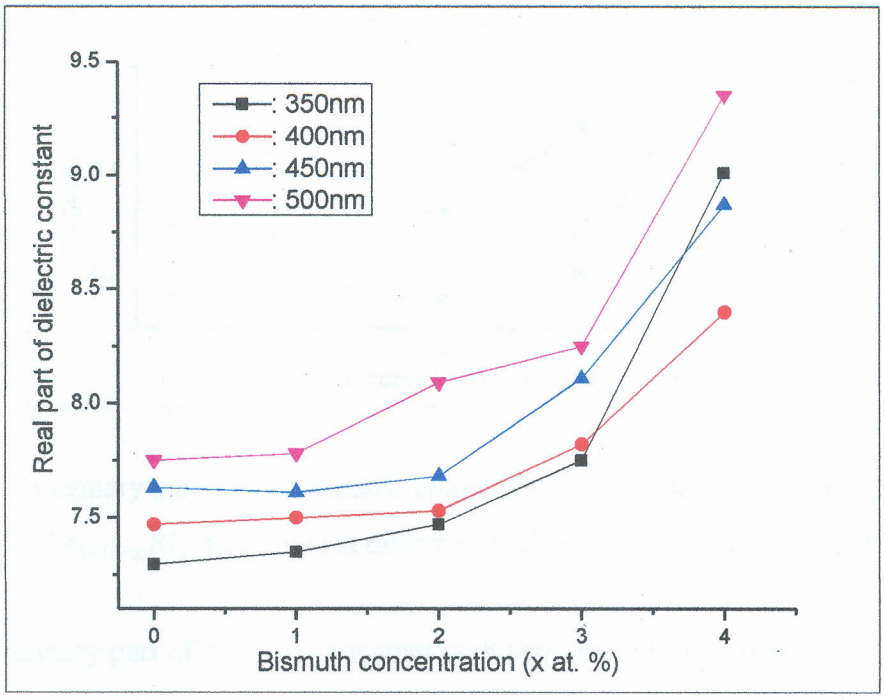

Figure 4.11: Real part of the dielectric constant against bismuth concentration ($x\ at.\%$) for $Se_{100-x}Bi_x$ thin films at different thicknesses, wavelength, $\lambda = 750nm$

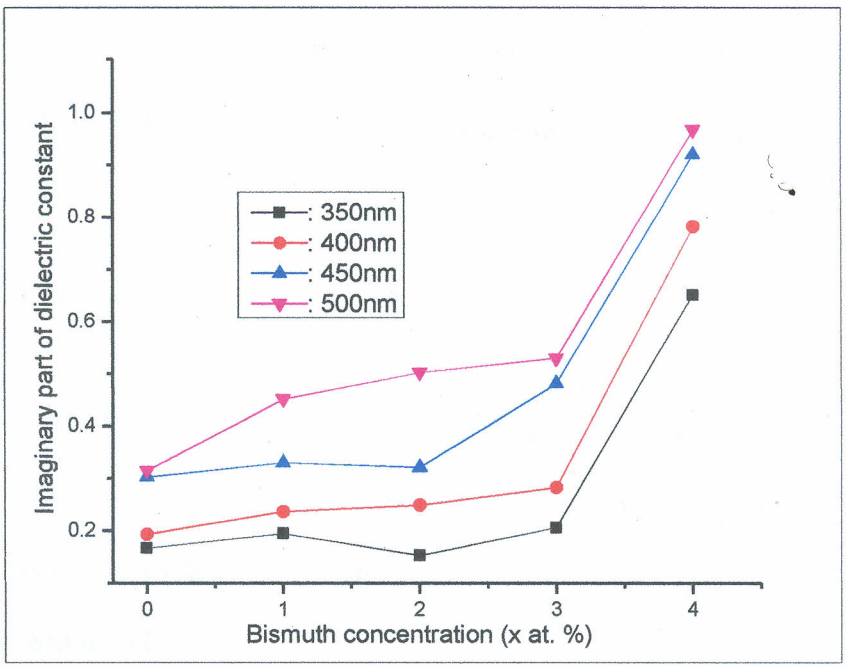

Figure 4.12: Imaginary part of the dielectric constant against bismuth concentration ($x\ at.\%$) for $Se_{100-x}Bi_x$ thin films at different thicknesses and wavelength, $\lambda = 750nm$

Increase in imaginary part of dielectric constant with bismuth concentration of the deposited thin films is observed in figure 4.12. In addition, the imaginary part increases with increase in film thickness due to the effect of the extinction coefficient. This is because the imaginary part of dielectric constant is proportional to the extinction coefficient with respect to equation (4.4). As a result, there is a corresponding increase in the imaginary part of the dielectric constant with film thickness. For a 350nm thin film,$0.167 \leq \varepsilon_2 \leq 0.651$, $0.193 \leq \varepsilon_2 \leq 0.782$ for 400nm, $0.303 \leq \varepsilon_2 \leq 0.920$ for 450nm, and $0.315 \leq \varepsilon_2 \leq 0.968$ for 500nm.

4.7 Optical band gap energy of the deposited thin films

The band gap energy of a semiconductor is the minimum energy needed to move an electron from its bond state within an atom to a free state. This Free State is where the electron can be

involved in conduction process. It is the energy difference between the conduction band and the valence band of the semiconductor material. To obtain the optical band gap energy of the deposited $Se_{100-x}Bi_x$ $(x = 0, 1, 2, 3\ and\ 4\ at.\%)$ thin films from figure 4.13, equation (4.1) was used;

$$(\alpha h\nu)^{1/2} = (h\nu - E_g) \tag{4.1}$$

This equation was derived from equation $(2.7b)$) for $\gamma = 2$ according to *Tauc* proposal for most amorphous semiconductors [61]. This was made possible by extrapolating the graph to the energy axis. Other researchers have also found selenium rich binary and ternary glasses to obey the indirect rule transition [11, 12, 54, 56].

The equation (4.1) is a straight line equation, though the graphs do not touch $x - axes$ and this is because the absorption coefficient for the selenium-bismuth thin films in the region under investigation (visible region) is not zero. Further, the range of wavelength used was 200nm-3000nm and not from zero. This has already been explained in the methodology section. As a result, energy band gap is found only by extrapolating the curves to the energy axis as shown by the dotted lines in figure 4.13. The optical band gap energy from figure 4.13 decreased with bismuth addition. Similar trend has been observed by other authors [11, 12, 62, 63].

Figure 4.13 show graphs of $(\alpha h\nu)^{1/2}(eVcm^{-1})^{1/2}$ against photon energy (eV).

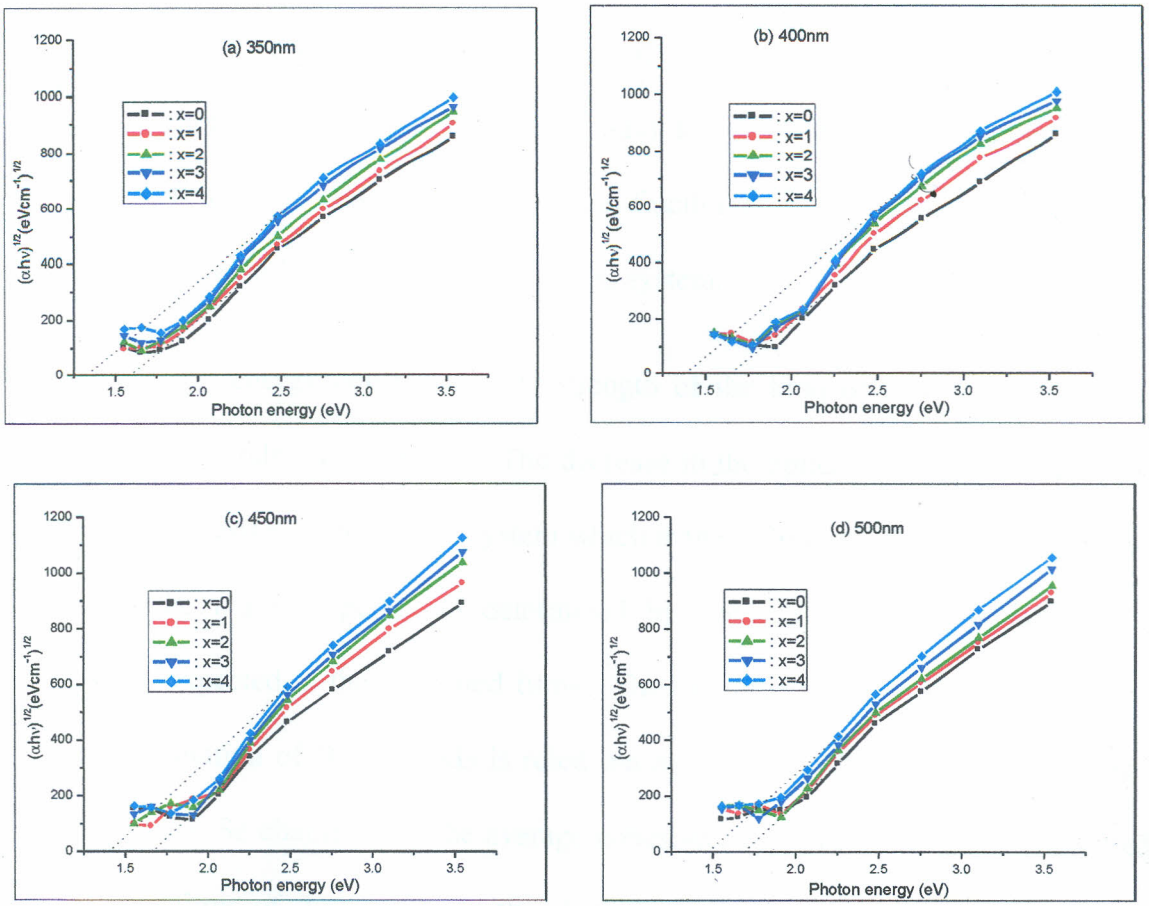

Figure 4.13: $(\alpha hv)^{1/2}(eVcm^{-1})^{1/2}$ against photon energy (eV) for $Se_{100-x}Bi_x$ thin films at different film thicknesses; (a) 350nm, (b) 400nm, (c) 450nm and (d) 500nm

The band gap energy decreased from $1.352eV$ to $1.263eV$ for 350nm thin films, $1.425eV$ to $1.251eV$ for 400nm thin films, $1.501eV$ to $1.275eV$ for 450nm thin films and from $1.676eV$ to $1.289eV$ for 500nm thin films. When bismuth is added to selenium, it introduces defect states in the amorphous selenium glass structure and this reduces the optical band gap energy of the system. Introduced bismuth atoms leads to the formation of the heteropolar Se-Bi bonds (bond energy 40.7kcalmol^{-1}) at the expense of the homopolar Se-Se bonds (bond energy 44.4kcalmol^{-1}) [19]. This leads to a decrease in the concentration of Se-Se bonds. Therefore, increasing the

concentration of Bi atoms in the $Se_{100-x}Bi_x$ system could decrease the glass bond energies and consequently its optical energy gap. The number of Se-Bi bonds increase with increase in bismuth concentration. In addition, bismuth is said to partly break the Se_8 ring structure (covalently bonded) and this may increase the chain fraction (Van der Waals bonded) [62, 64], that could lead to decreased optical energy gap of the system.

The optical band gap energy depends on the strength of the kind of bond that exists in the $Se_{100-x}Bi_x$ thin films under consideration. The decrease in the optical band gap energy may be due to decrease in cohesive energy of the system which is the stabilization energy of an infinitely large cluster of the material per atom determined by summing the bond energies of the consequent bonds expected in the deposited films. The expected bonds in this study are Se-Se and Se-Bi. The formation of Bi-Bi bonds is ruled out as it is argued that their bond energy is lower than that of the Se chains [65]. The average cohesive energy of all the bonds expected in the deposited thin films of $Se_{100-x}Bi_x$ is therefore low, leading to reduced optical band gap energy. This is because the optical band gap energy is sensitive to the bond energy [66].

Band gap energy against bismuth concentration ($x\ at.\%$) for $Se_{100-x}Bi_x$ thin films at different film thickness at wavelength, $\lambda = 750nm$ is shown in figure 4.14. We note that the band gap energy of the deposited thin films of selenium-bismuth slightly increases from $x = 0\ at.\%$ to $x = 1\ at.\%$ and then decreases with increase in bismuth concentration. The increase may be due to shift in Fermi level and the decrease may be due to increase in density of defect states in the deposited thin films as observed by *Davis and Mott* [37].

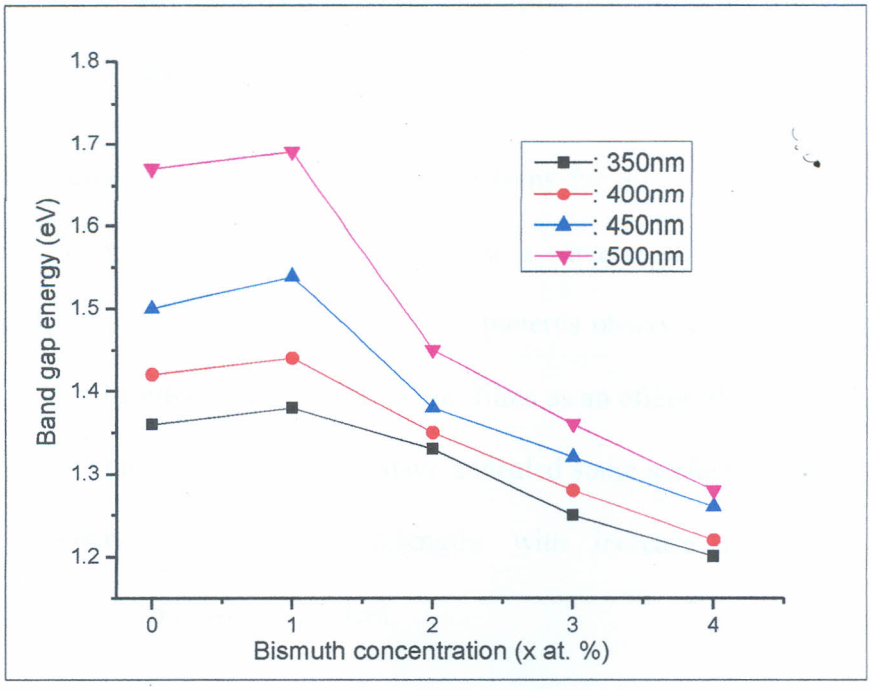

Figure 4.14: Band gap energy against bismuth concentration ($x\ at.\%$) for $Se_{100-x}Bi_x$ thin films at different film thicknesses and wavelength, $\lambda = 750nm$

The band gap energy of the deposited $Se_{100-x}Bi_x$ thin films varies with film thickness due to high density of dislocations resulting from bismuth impurity in the system. Since dislocation density increases with increase in film thickness, it is expected that high dislocation density leads to increase in band gap energy as the film thickness increases. Greater deposition generally builds up more homogenous network which minimizes the number of defects and the localized states thereby increasing the electronic band gap energy [67]. The energy band gap increased from $1.263eV$ for 350nm thin films to $1.676eV$ for 500nm thin films. This means that thin films with a thickness of 350nm are best for the formation of solar cell modules compared to the thick films. Therefore, in the analysis of effect of substrate temperature on the optical properties of selenium-bismuth thin films, we narrow down to the 350nm thin films.

4.8 Effect of substrate temperature on the optical properties of deposited 350nm $Se_{100-x}Bi_x$ thin films

Transmittance spectra for $350nm\ Se_{100-x}Bi_x$ thin films for different substrate temperature are shown in figure 4.15. Transmission of light below a wavelength of 500nm was zero as this represents the absorption region. The interference patterns observed in figure 4.15 indicates the homogeneity and uniformity of the deposited thin films as an effect of the substrate temperature. This is because substrate temperature may have annealed some surface defects in the films. The transmittance decreased for fixed wavelengths with increase in substrate temperature (51°C, 55°C, *and* 59°C) and bismuth content.

The transmittance against substrate temperature (°C) for $350nm\ Se_{100-x}Bi_x$ thin films at wavelength, λ = 750nm is shown in figure 4.16. The transmittance decreased from 0.667 (at 51°C, $x = 0\ at.\%, \lambda = 750nm$) to 0.542 (at 59°C, $x = 0\ at.\%, \lambda = 750nm$) from figure 4.16. This is due to scattering and reflection of light. Interference maxima and minima due to multiple reflections on film surfaces can be observed, an indication of the thickness uniformity of the thin films. In the low wavelength region, the transmittance was low due to light absorption.

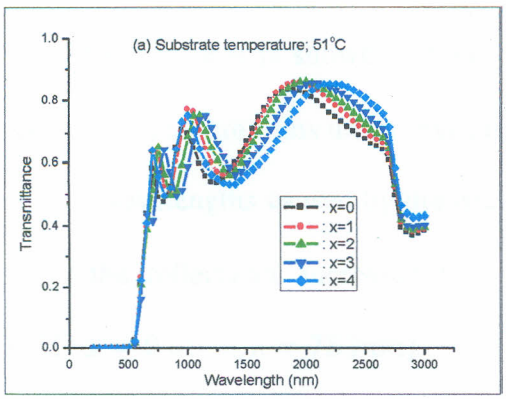

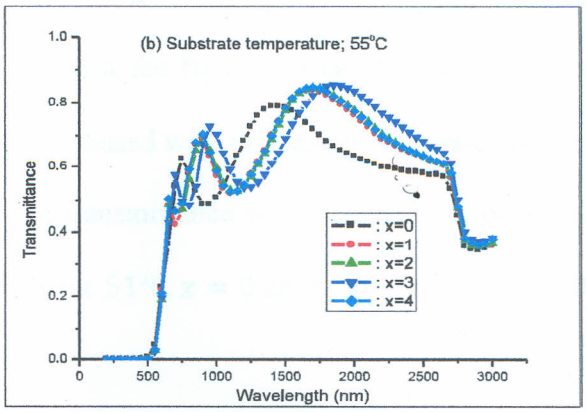

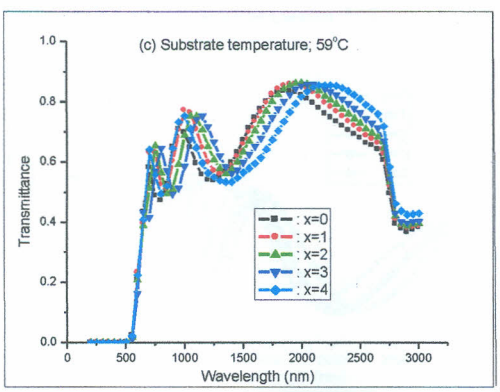

Figure 4.15: Transmittance against wavelength (nm) for $350nm\ Se_{100-x}Bi_x$ thin films at different substrate temperatures; (a) 51°C, (b) 55°C and (c) 59°C.

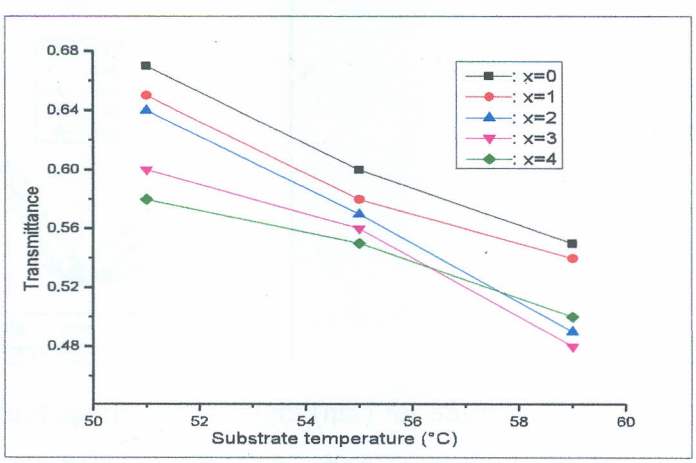

Figure 4.16: Transmittance against substrate temperature (°C) for $350nm\ Se_{100-x}Bi_x$ thin film at wavelength, $\lambda = 750$nm

The spectral dependence of reflectance for the $350nm\ Se_{100-x}Bi_x$ thin films at different substrate temperatures is shown in figure 4.17. From the figures, it can be observed that the reflectance for the thin films under investigation increased with increase in substrate temperature at specific wavelengths caused by the decrease in transmittance with substrate temperature. For example, the reflectance increased from 0.315 (at $51°C, x = 0\ at.\%, \lambda = 750nm$) to 0.450 (at $59°C,\ x = 0\ at.\%, \lambda = 750nm$).

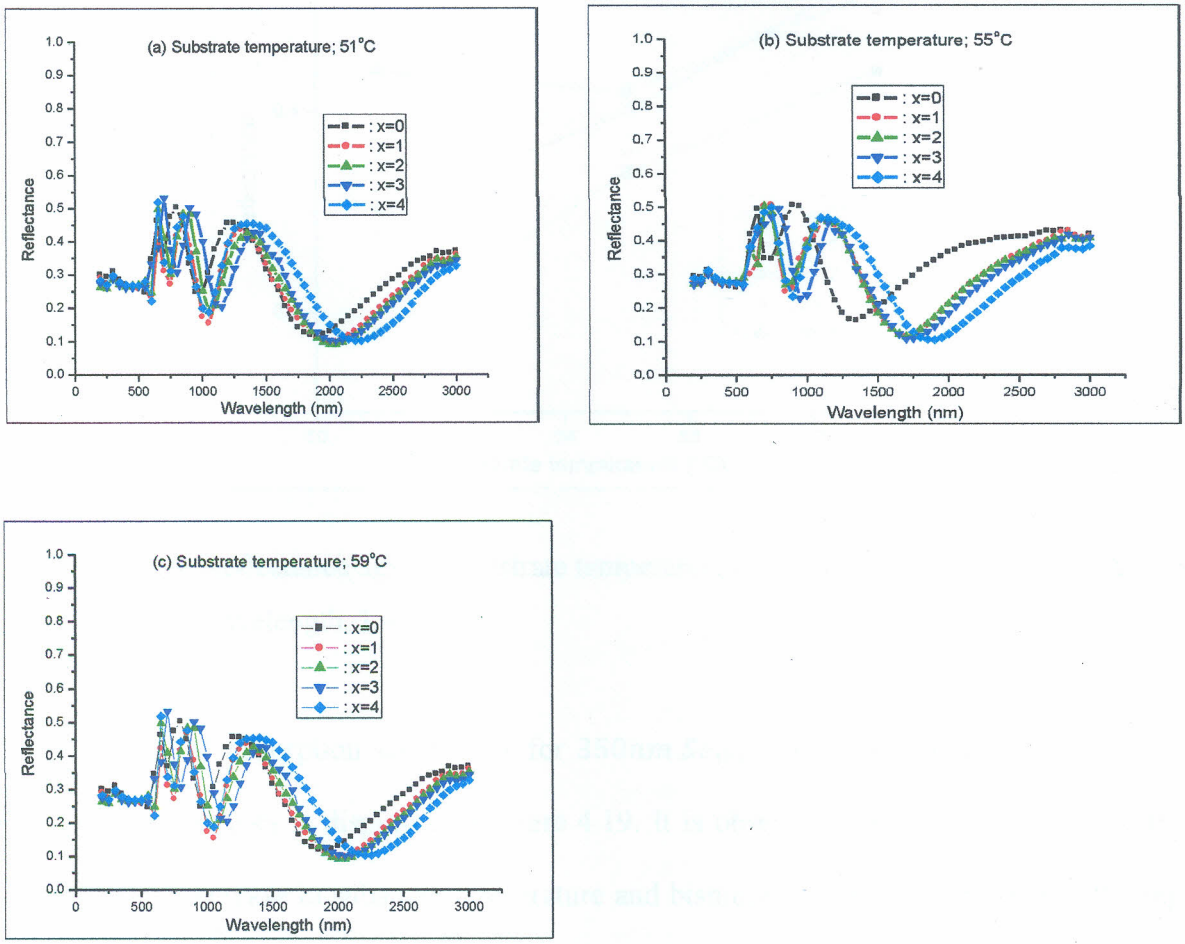

Figure 4.17: Reflectance against wavelength (nm) for $350nm\ Se_{100-x}Bi_x$ thin films at different substrate temperatures; (a) 51°C, (b) 55°C and (c) 59°C.

The reflectance against substrate temperature (°C) for $350nm\ Se_{100-x}Bi_x$ thin films at wavelength, λ = 750nm is shown in figure 4.18. The reflectance values are low compared to those for the same 350nm thin films at room temperature from section 4.2. This means the films are less reflecting. This is a best property for a material to be used for thin film solar cells.

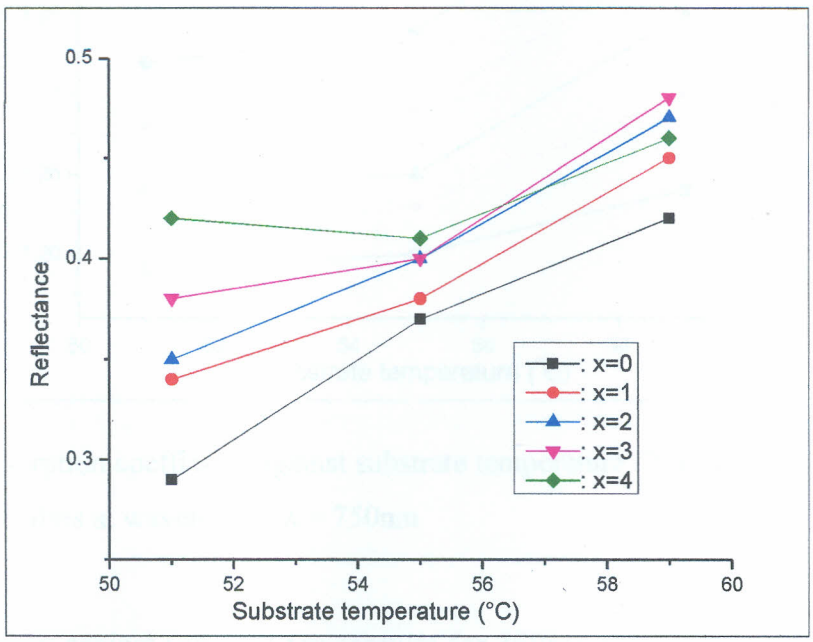

Figure 4.18: Reflectance against substrate temperature (°C) for $350nm\ Se_{100-x}Bi_x$ thin films at wavelength, λ = 750nm

The variation of absorption coefficient for $350nm\ Se_{100-x}Bi_x$ thin films grown at different substrate temperatures is displayed in figure 4.19. It is observed that the absorption coefficient increases with increase in substrate temperature and bismuth content. This consequently implies reduction in transmittance of the films [55]. The values of the absorption coefficient are of order $\geq 10^4 cm^{-1}$ in the investigated spectral range, and this is good for thin film solar cell formation.

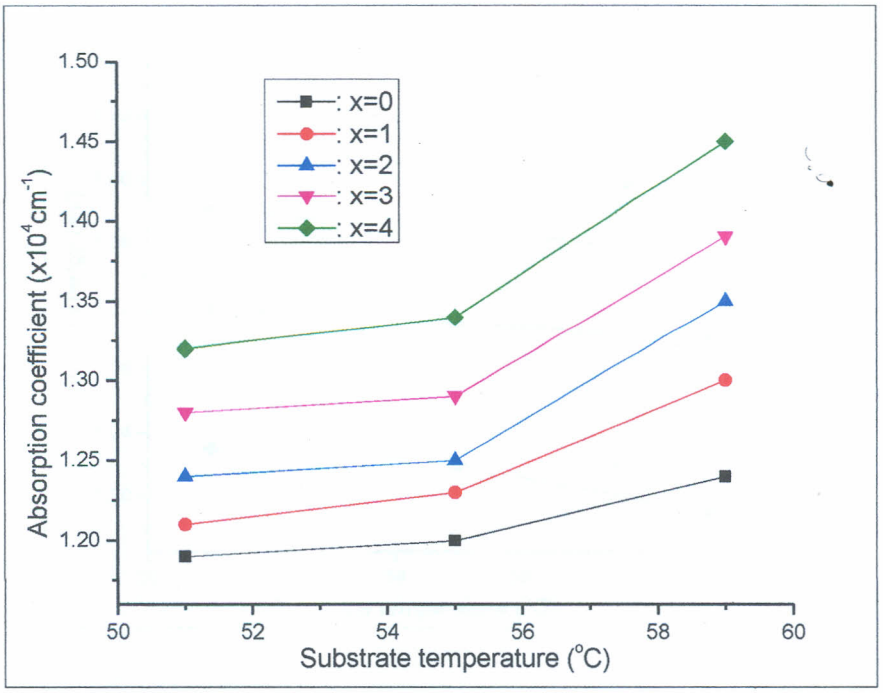

Figure 4.19: Absorption coefficient against substrate temperature (°C) for $350nm\ Se_{100-x}Bi_x$ thin films at wavelength, λ = 750nm

The band gap energy against substrate temperature for $350nm\ Se_{100-x}Bi_x$ thin films is shown in figure 4.20. Indirect optical band gap energy from the figure was found to decrease with increase in substrate temperature and bismuth content. This trend has also been observed by [67] while studying $CuGa_{0.25}In_{0.75}Se_2$ amorphous thin films. Reduction in optical band gap energy of the deposited thin films can be understood in terms of *Davis-Mott model*, according to which, decrease in band gap energy is a consequence of increase in disorder in the deposited amorphous thin films due to bismuth content [37]. The disorder could also have come from point defects which are either 'frozen in' during the quench from a molten state or grown during deposition [55].

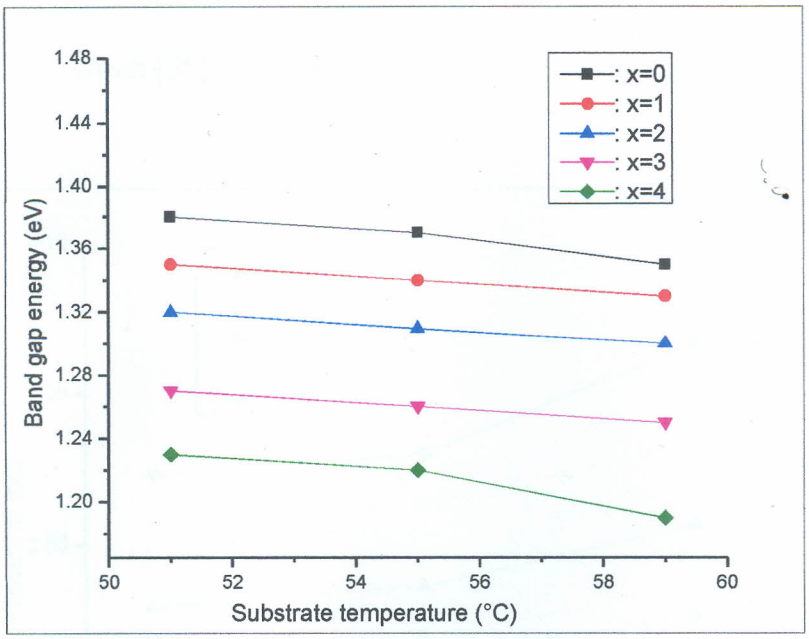

Figure 4.20: Band gap energy (eV) against substrate temperature (°C) for $350nm\ Se_{100-x}Bi_x$ thin films at wavelength, λ = 750nm

Refractive index against substrate temperature for $350nm\ Se_{100-x}Bi_x$ thin films is shown in figure 4.21. It is observed from the figure that as the substrate temperature and bismuth content increased, the refractive index increased. This means that the refractive index depends on the polarizability of the system which further depends on the covalent radius of atoms of the elements (*Selenium and Bismuth*) under consideration. Since the atomic radius of bismuth is greater than that of selenium, its polarizability is higher than that of selenium according to Lorentz-Lorenz relation [12, 68];

$$\frac{n^2-1}{n^2+2} = \frac{1}{3\varepsilon_0}\sum_i N_i \alpha_{pi} \tag{4.6}$$

where ε_o is the vacuum permittivity, N_i is the number of polarisable units of type i per unit volume with polarizability α_{pi}.

Therefore, the refractive index shows its dependence on the composition of films. This agrees well with the work of *Alwan* [55].

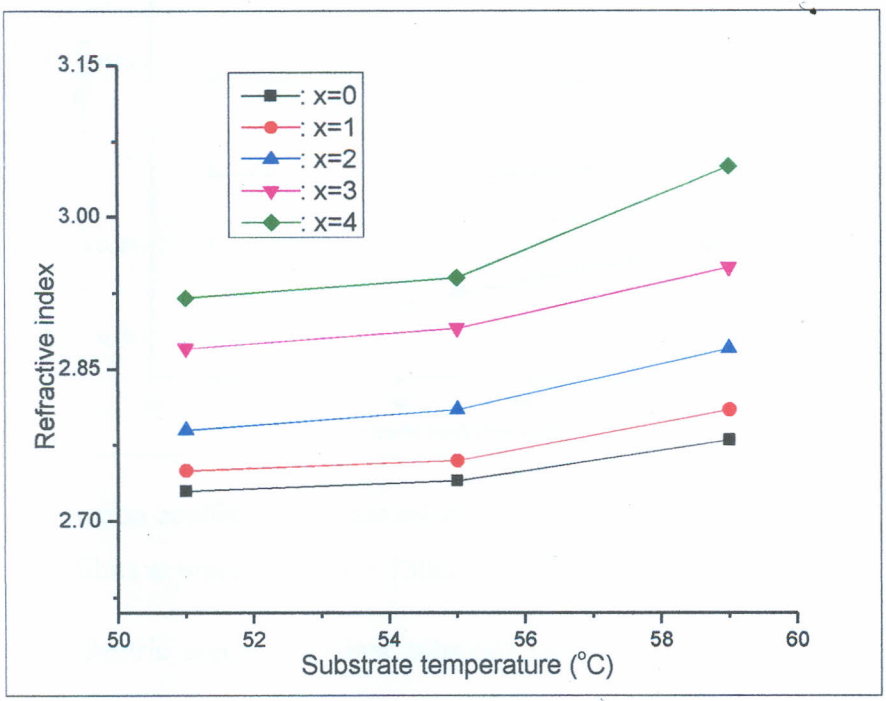

Figure 4.21: Refractive index against substrate temperature (°C) for $350nm\ Se_{100-x}Bi_x$ thin films at wavelength, λ = 750nm

The plot of extinction coefficient against substrate temperature is shown in figure 4.22. It is clear that the extinction coefficient of the deposited thin films increases with increase in substrate temperature due to the effect of absorption coefficient of the films. The general low values of extinction coefficient in the order of 10^{-2} in the visible region may be a qualitative indication of excellent surface smoothness of the $350nm\ Se_{100-x}Bi_x$ thin films. This behaviour of increase of extinction coefficient with substrate temperature is an indication of the low transmittance observed in the visible region at specific wavelengths.

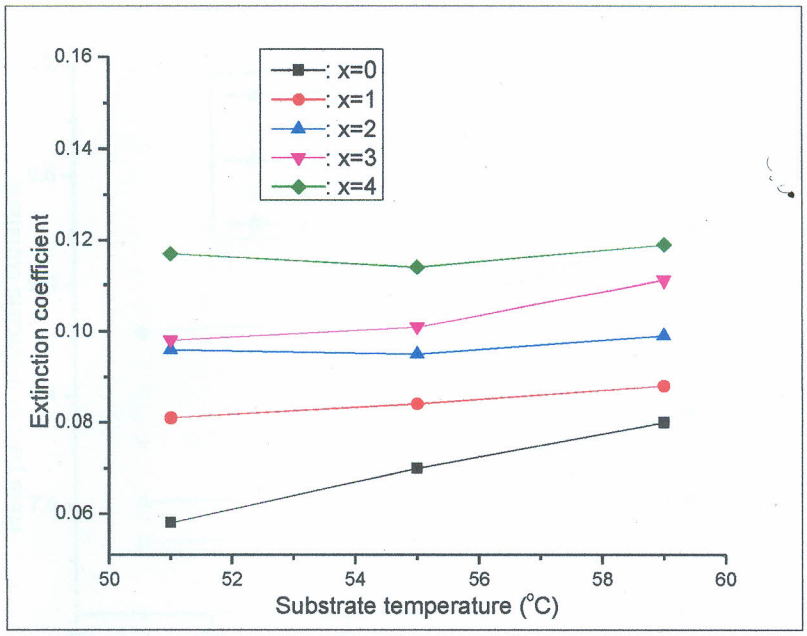

Figure 4.22: Extinction coefficient against substrate temperature (°C) for $350nm\ Se_{100-x}Bi_x$ thin films at wavelength, λ = 750nm

The real part of dielectric constant against substrate temperature (°C) for $350nm\ Se_{100-x}Bi_x$ thin films at wavelength, λ = 750nm is shown in figure 4.23. The variation of real part of the dielectric constant with substrate temperature corresponds to the graph of refractive index versus substrate temperature. Figure 4.23 of variation of real part of the dielectric constant with substrate temperature corresponds to the graph of refractive index versus substrate temperature. This is because the real part of dielectric constant is proportional to the refractive index of the selenium-bismuth thin films. This is in line with equation 4.4; hence, refractive index manifests itself in the real part of dielectric constant.

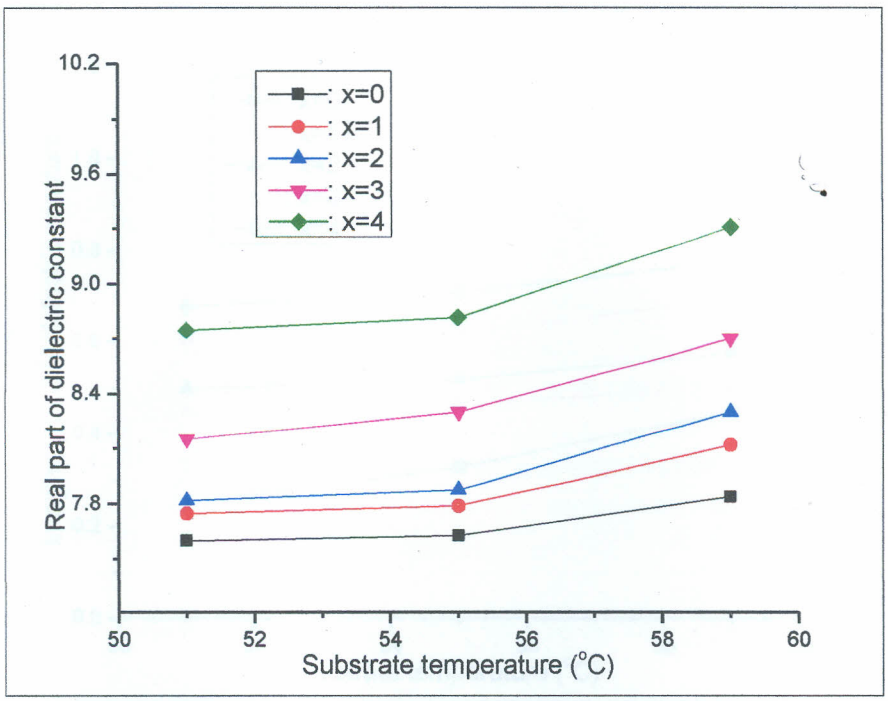

Figure 4.23: Real part of dielectric constant against substrate temperature (°C) for $350nm\ Se_{100-x}Bi_x$ thin films at wavelength, λ = 750nm

Figure 4.24 corresponds to the graph of extinction coefficient versus substrate temperature. This is in line with equation 4.4. Increase in imaginary part of the dielectric constant is an indication of increase in absorption coefficient with increase in substrate temperature. This implies that the deposited thin films of selenium-bismuth alloy thin films are sensitive to light.

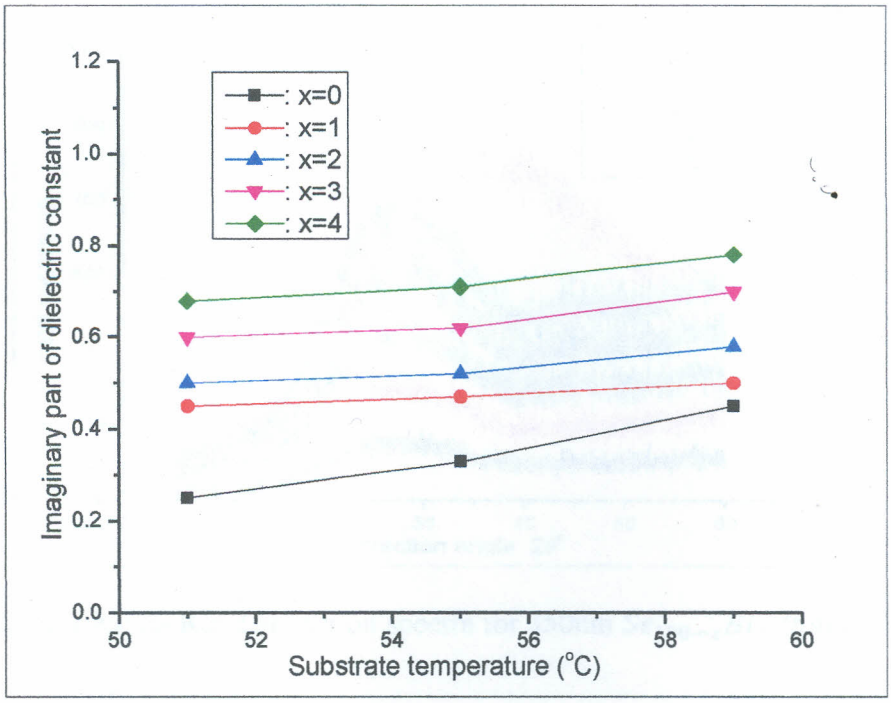

Figure 4.24: Imaginary part of dielectric constant against substrate temperature (°C) for $350nm\ Se_{100-x}Bi_x$ thin films at wavelength, λ = 750nm

4.9 X-Ray Diffraction analysis for the deposited thin films

X- Ray Diffraction spectra for 350nm $Se_{100-x}Bi_x$ thin films at a substrate temperature of 59°C are shown in figure 4.25. From the figure, X-Ray Diffraction Spectra of the $Se_{100-x}Bi_x$ thin films of thickness $350 \pm 10nm$ revealed that the deposited films are amorphous in nature as no prominent peak was observed in their spectra. Absence of any sharp peaks in X- Ray Diffraction patterns confirmed the glassy nature of $Se_{100-x}Bi_x$ thin films [18, 29]. This simply means that the grain size of the films was very small and that the disorder within these grains was so high that no specific diffraction peaks could be detected. The observed humps in figure 4.25 are the effect of the glass substrate. Presence of humps in the XRD spectra is verification of small to medium range order in amorphous thin films [56].

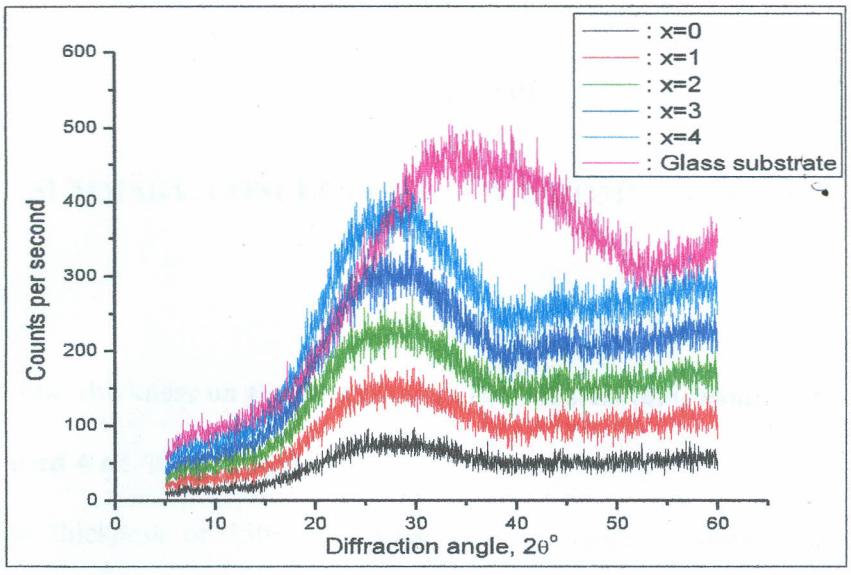

Figure 4.25: X- Ray Diffraction spectra for 350nm $Se_{100-x}Bi_x$ thin films

4.10 A comparison of the investigated optical properties of $Se_{100-x}Bi_x$ thin films with published work

Table 4.1 compares this work with already published work

Material	x	n	k	E_g eV	$\alpha \times 10^4 cm^{-1}$	Ref.
$Se_{100-x}Bi_x$	0, 1, 2, 3, 4	2.722 -2.963	0.028-0.093	1.263-1.352	1.641-2.011	This study
$Se_{100-x}Bi_x$	0.0, 0.5, 2.5, 5.0	2.25-2.68	0.158-0.197	1.12-1.61	2.76-3.44	[11]
$Te_{15}(Se_{100-x}Bi_x)_{85}$	0, 1, 2, 3, 4, 5	2.95-3.54	0.059-0.072	1.21-1.37	-	[12]

Table 4.1: A comparison of investigated thin films with published work

The main cause of the variation is to do with the varied deposition methods [13].

CHAPTER FIVE

SUMMARY, CONCLUSIONS AND RECOMMENDATIONS

5.1 Summary

A. Effect of film thickness on the optical properties of selenium-bismuth, $Se_{100-x}Bi_x(x = 0, 1, 2, 3 \text{ and } 4 \text{ at.}\%)$ thin films.

i. A film thickness of 350±10nm gave the best range of optical band gap energy of $1.263eV - 1.352eV$ which decreased with increase in bismuth content.

ii. All the films of different film thicknesses (350±10nm, 400±10nm, 450±10nm and 500±10nm) exhibited high absorption coefficient in the order of $10^4 cm^{-1} - 10^5 cm^{-1}$ especially in the visible region.

iii. Some absorption in the infrared region of wavelength ≥900nm in the order of $10^2 cm^{-1}$ was observed.

B. Effect of substrate temperature on the optical properties of 350±10nm selenium-bismuth, $Se_{100-x}Bi_x(x = 0, 1, 2, 3 \text{ and } 4 \text{ at.}\%)$ thin films.

i. Improved optical band gap energy in the range $1.381eV - 1.462eV$ was observed and decreased with increase in substrate temperature.

ii. Transmittance reduced with increase in substrate temperature from 0.67 to 0.55. Further, the transmittance spectra shifted towards higher wavelengths in the visible region.

iii. Successfully deposited thin films of selenium-bismuth at substrate temperatures 51°C, 55°C and 59°C without crystallization, yet glass transition temperature for amorphous selenium thin films is just 42°C.

iv. The films exhibited high absorption coefficient in the order of $10^4 cm^{-1} - 10^5 cm^{-1}$ especially in the visible region. In addition, some absorption in the infrared region of wavelength ≥900nm in the order of $10^2 cm^{-1}$ was also observed.

5.2 Conclusions.

i. The range of optical band gap energy of $1.263eV - 1.352eV$ and $1.381eV - 1.462eV$ means that the selenium-bismuth alloy thin films can readily absorb photons in the sunlight and change them to electricity. The best optical band gap energy was observed at the highest bismuth content i.e. $x = 4\,at.\%$ at $1.352eV$ and $1.462eV$ for the 350±10nm. This is within optimized optical band gap energy for a solar cell thin film of about $1.4eV - 1.5eV$.

ii. The high absorption coefficient in the order of $\geq 10^4 cm^{-1}$, the reduced transmittance and the observed shift in the transmittance spectra towards higher wavelengths within the visible region with increase in substrate temperature in selenium-bismuth alloy thin films is an indication of photosensitive thin films.

iii. The observed absorption coefficient in the infrared region of $10^2 cm^{-1}$ at different film thickness and substrate temperature implies that the deposited selenium-bismuth alloy thin films are sensitive in the infrared region. Formation of amorphous thin films of selenium-bismuth at a substrate temperature of 59°C without forming crystals is an indication of increased crystallization temperature and stability for the deposited thin films.

5.3 Recommendations.

A. Applications of deposited selenium-bismuth, $Se_{100-x}Bi_x$ thin films based on this study.

i. The high absorption coefficient obtained for the 350±10nm selenium-bismuth alloy thin films which is $\geq 10^4 cm^{-1}$ with optimized optical band gap energy in the range $1.263eV - 1.462eV$, the produced thin films can be used to make thin film solar cells with high solar conversion efficiency. This is because the deposited thin films are photosensitive in the visible region. This will improve the life of a common Kenyan both in the rural and urban environment.

ii. Films formed by combining the metal bismuth with selenium have been found to be sensitive to infrared radiation and may, therefore, be employed in xerographic systems receiving radiation which is out of the visible spectrum. Films of bismuth and selenium may also be employed as the photoconductor layer for use in the flat panel x-ray image detector and high definition digital and video camera.

iii. Addition of bismuth to selenium improves the crystallization temperature and stability. Therefore, selenium-bismuth based alloys are thought to be promising media, which makes use of a phase change between an amorphous state and a crystalline state and are used to extend the utility of amorphous selenium films in threshold switch devices and in the production of compact disks for information storage.

B. Further studies

i. There is need to study the surface morphology of $Se_{100-x}Bi_x$ thin films and investigate its effect on the optical and electrical properties of the deposited films.

ii. The study concentrated on the optical characterization of deposited $Se_{100-x}Bi_x$ ($x = 0, 1, 2, 3\ and\ 4\ at.\%$) thin films without further treatment. There is need to investigate the

effect of annealing of the films in both vacuum and air on the optical properties of the films.

iii. The study focused on the optical properties of the deposited $Se_{100-x}Bi_x$ $(x = 0, 1, 2, 3\ and\ 4\ at.\%)$ thin films. Further measurements of other optical properties and mechanical ones need investigation as well. These include the photo-darkening, photo-bleaching, photo-contraction and photo-expansion. The Bismuth concentration can also increase beyond $x = 4\ at.\%$.

REFERENCES

[1] Shinnar R. and Citro F., *Sustainable fuel for the transportation sector*, Proceedings of National Academic Science, USA, 20th March, (2007), pp. 4828-4833

[2] Waiguru A., Cabinet Secretary, Ministry of Devolution and Planning, *Economic survey 2013 highlights,* Proceedings of the National Survey, Nairobi, Kenya, May, (2013), pp.26-29

[3] Luque A. and Hegedus S., *Handbook of Photovoltaic Energy Conversion and Engineering*; John Wiley & Sons Ltd, Chichester, West Sussex, England, (2003), pp. 3-22

[4] Green M. A., Emery K., Hishikawa Y., and Warta W., *Solar Cell Efficiency tables (Version 35), In: Progress in Photovoltaics,* Research and Applications, Vol. 18, (2010), pp. 144-150

[5] Zhang Z., Witte W., Kiowski O., Lemmer U., Powalla M., and Holscher H., *Influence of the Ga content on the optical and electrical properties of* $CuIn_{1-x}Ga_xSe_2$ *thin film solar cells*, Photovoltaics, IEEE, Vol. PP, Issue 99, (2012), pp. 1-5

[6] Mohd N. and Zulfequar M., *DC Conductivity and dielectric behaviour of glassy* $Se_{100-x}Zn_x$ *alloy* Journal of Inorganic Non-Metallic Materials, Vol. 2, (2012), pp. 11-17

[7] Elliot S. R., *Chalcogenide glasses*. In: Zarzycki J. (ed.), *Materials Science and Technology*, VCH, New York, (1991), pp. 375-454

[8] Green M. A., Emery K., Bucher K., King D. L., and Igari S., *Solar cell Efficiency Tables (Version 12), In: Progress in Photovoltaics*, Research and Applications, Vol. 6, Issue 4, (1998), pp. 265-270

[9] Popescu M., *Self-organization in amorphous semiconductors and chalcogenide glasses,* Journal of Advanced Materials, Vol. 8, No. 6, (2006), pp. 2164-2168

[10] Soltan A. S., Abu El-Oyoun M., Abu-Sehly A. A., and Abdel-Latief A. Y., *Thermal annealing dependence of the structural, optical and electrical properties of selenium-tellurium films*, Materials Chemistry and Physics, Vol. 82, (2003), pp. 101-106

[11] Majeed Khan M. A., Zulfequar M., and Husain M., *Optical investigation of a-*$Se_{100-x}Bi_x$ *alloys,* Optical Materials, Vol. 22, (2003), pp. 21-29

[12] Kumar K., Sharma P., Katyal S. C., and Thakur N., *Optical parameters of ternary* $Te_{15}(Se_{100-x}Bi_x)_{85}$ *thin films deposited by thermal evaporation*, Phys. Scr. Vol. 84, No. 045703, (2011), pp. 1-6

[13] Marquez E., Bernal-Oliva A. M., Gonzalez-Leal J. M., Prieto-Alcon R., Ledesma A., Jimenez-Garay R., and Martil I., *Optical constant calculation of non-uniform thickness*

thin films of the $Ge_{10}As_{15}Se_{75}$ chalcogenide glassy alloy in the sub-band gap region $(0.1 - 1.8eV)$, Materials Chemistry and Physics, Vol. 60, No. 3, (1999), pp. 231-239

[14] Sissoko G., Museruka C., Correa A., Gaye I., and Ndiaye A. L., *Light spectral effect on recombination parameters of silicon solar cell*, Proceedings of the World Renewable Energy Congress, Denver-USA, Part III, 29th June, (1996), pp. 1487-1490

[15] Borisova Z. U., *Glassy Semiconductors*, *7th Ed.*, Plenum Press, New York, (1981), pp. 400 506

[16] Schardt R. C., *Photodarkening of Germanium – Selenium Glasses Induced by Below Band gap Light*, Ph.D. dissertation, University of Florida, USA, (2000), pp.28-179

[17] Zallen R., *The Physics of Amorphous Solids*, John Wiley & Sons, New York, (1983), pp. 60- 200

[18] Bindu K., Lakshmi M., Bini S., Sudha kartha C., Vijayakumar K. P., Abe T., and Kashiwaba Y., *Amorphous selenium thin films prepared using chemical bath deposition: Optimization of the deposition process and characterization*, Semiconductor Science and Technology, Vol. 17, No. 3, (2002), pp. 270-274

[19] Hafiz M. M., El-Shazly O., and Kinawy N., *Reversible phase change in Bi_xSe_{100-x} chalcogenide thin films for use as optical recording medium*, Applied Surface Science, Vol. 171, (2001), pp. 231-241

[20] Saitar J. M., Ledru J., Hamou A., and Saffarini G., *Crystallization of As_xSe_{1-x} from the glassy state* $(0.005 < x < 0.03)$, Physica B, 245, (1998), pp. 256-262

[21] Street R. A. and Mott N. F., *States in the gap of glassy semiconductors*, Physical Review Letters, Vol. 35, No. 19, (1975), pp. 1293-1296

[22] Malik M. M., Zulfequar M., Kumar A., and Husain M., *Effect of Indium impurities on the electrical properties of amorphous $Ga_{30}Se_{70}$* , Journal of Physics: Condensed Matter, Vol. 4, No.43, (1992), pp. 8331-8338

[23] Yadav S., Sharma S. K., Dwivedi P. K., and Kumar A., *Determination of D. C conduction parameters in $a - Se_{100-x}Bi_x$ thin films*, Journal of Non-Oxide Glasses, Vol. 3, No.1, (2011), pp. 17-24

[24] Ji K., Pal R. K., Agnihotri A. K., Shukla R. K., and Kumar A., *Space Charge Limited Conduction in Glassy $Se_{100-x}Bi_x$ Alloys*, Chalcogenide Letters, Vol. 6, No. 2, (2009), pp. 77-81

[25] Majeed Khan M. A., Kumar S., Husain M. and Zulfequar M., *Dielectric studies on $a - Se_{100-x}Bi_x (x = 0, 0.5, 2.5, 5 \& 10\ at.\%)$ system*, Journal of Non-Oxide Glasses, Vol. 1, No. 1, (2009), pp. 71-80

[26] Ji K., Pal R. K., Agnihotri A. K, Shukla R. K., and Kumar A., *A comparative study of the density of defect states in thin films and bulk samples of glassy* $Se_{100-x}Bi_x$, Journal of Ovonic Research, Vol. 5, No. 3, (2009), pp. 71-76

[27] Majeed Khan M. A., Zulfequar M., and Husain M., *Estimation of Density of Localized State of* $Se_{100-x}Bi_x$ *films from electrical properties*, Physica B, Netherland, Vol. 322, (2002), pp.1-11

[28] Srivastava S., Zulfequar M., and Kumar A., *Study of glass transition kinetics in glassy alloys of* $Se_{100-x}Bi_x$, Chalcogenide Letters, Vol. 6, No. 8, (2009), pp. 403-414

[29] Majeed Khan M. A., Kumar S., Husain M., and Zulfequar M., *Thermal Properties of Selenium-Bismuth Glassy Alloys*, Chalcogenide Letters, Vol.4, No.12, (2007), pp. 147-153

[30] Kumar K., Thakur N., Katyal S. C., and Sharma P., *A study of the physical properties of* $Te_{15}(Se_{100-x}Bi_x)_{85}$ *Glassy alloy,* Defect and Diffusion Forum, Vol. 305/306, (2010), pp. 61-69

[31] Pandey V., Tripathi S. K., and Kumar A., *Optical properties of amorphous* $Se_{100-x}Sb_x$ *thin films,* Journal of Ovonic Research, Vol. 2, No. 4, (2006), pp. 67-76

[32] Fouad S. S., Ammar A. H., and Abo-Ghazala, *Optical properties of* Sb_xSe_{1-x} *thin films*, Physica B, Vol. 229, (1997), pp. 249-251

[33] Sharma P., Sharma I., and Katyal S. C., *Physical and optical properties of binary amorphous selenium-antimony thin films,* Journal of Applied Physics, Vol. 105, No. 053509, (2009), pp.1-7

[34] Malinovsky V. K. and Surovtsev N. V., *Optical memory in chalcogenide glasses*, Chalcogenide Letters. Vol. 9, No. 2, (2012), pp. 79-84

[35] Tanaka K., *Mechanisms of photo-darkening in amorphous Chalcogenides*, Journal of Non-Crystalline Solids, Vol. 59 & 60, (1983), pp. 925-928

[36] Anderson P. W., *Absence of diffusion in certain random lattices,* Physics Reviews, Vol.109, No.5, (1958), pp. 1492-1505

[37] Davis E. A. and Mott N. F., *Electronic Processes in Non-Crystalline Materials, 2nd Ed.* Clarendon Press, Oxford, (1979), pp. 382-455

[38] Emin D., Seager C. H., and Quinn R. K., *Small-Polaron hopping motion in some Chalcogenide glasses,* Physical Review Letters, Vol. 28, (1972), pp. 813-816

[39] Cohen M. H., Fritzsche H., and Ovshinsky S. R., *Simple band model for amorphous*

semiconductor alloys, Physical Review Letters, Vol. 22, (1969), pp. 1065-1068

[40] Ohring M., *The Material Science of Thin Films*, Academic Press, London, (2001), pp. 350-418

[41] Guenther R. D., *Modern Optics*, John Wiley & Sons, Singapore, (2001), pp. 64-300

[42] Born M. and Wolf E., *Principles of Optics, 7th Ed.*, Cambridge University Press-London, (1999), pp. 58-100

[43] Barman J., Sarma K. C., Sarma M., and Sarma K., *Structural and Optical Studies of Chemically Prepared CdS Nanocrystalline Thin Films*, Indian Journal of Pure and Applied Physics, Vol. 46, No. 5, (2008), pp. 339-343

[44] Morton D.E., *Characterizing optical thin films (I)*, Vacuum Technology and Coating, Vol. 2, No. 9, (2001), pp. 24-31

[45] Humphrey S., *Direct calculations of the optical constants for a thin film using a midpoint envelop*, Journal of Applied Optics, Vol. 46, No. 21, (2007), pp. 4660-4666

[46] Chopra K. L. and Malhotra L. K., *Thin Film Technology and Applications*, Tata McGraw Hill: New Delhi, India, Vol. 3, (1985), pp. 237-249

[47] Hemanadhan M., Bapanayya Ch., and Agarwal S. C., *Simple flash evaporation for making thin films of compounds*, Journal of Vacuum Science Technology, A 28 (4), (2010), pp. 625-626

[48] Soepardjo A. H., *$CuInSe_2$ thin film for solar cell by flash evaporation*, Makara, Sains, Vol. 13, No. 2, (2009), pp. 200-204

[49] Ramadan A. A., Abdel-Hady S., Abdel-Ghany S., and Soltan S. E., *Flash evaporation as an attempt for preparation of YBCO superconductor thin films*, Egyptian Journal of Solids, Vol. 23, No. 1, (2000), pp. 59-69

[50] Wei Z. G., Sandstorm R., and Miyazaki S., *TiNi-based thin film for MEMS applications*, Journal of Material Science, Vol. 33, (1998), pp. 3743-3746

[51] Miyazaki K. and Islam N., *Nanotechnology systems of innovation-An analysis of industry and academia research activities*, Technovation, Vol. 27, (2007), pp. 661-675

[52] Porter A. L., Roper A., Mason T., Rossini F., and Banks J., *Forecasting and management of technology*, Wiley, New York, pp. 435-442

[53] Swanepoel R., *Determination of the thickness and optical constants of amorphous silicon*, Journal of Physics E: Science Instrum. Vol. 16, (1983), pp. 1214-1218

[54] Shaaban E. R., Yahia I. S., and El-Metwally E. G., *Validity of Swanepoel's method for calculating the optical constants of thick films*, Acta Physica Polonica A, Vol. 121, No. 3, (2012), pp.628-635

[55] Alwan T. J., *The influence of substrate temperature on density of states and optical Properties of $Ge_{0.2}Te_{0.8}$ thin films*, Lebanese Science Journal, Vol. 12, No. 2, (2011), pp. 91-100

[56] Chauhan R., Tripathi A., Srivastava A. K., and Srivastava K. K., *Effect of swift heavy ion irradiation on optical and structural properties of amorphous $Ge - As - Se$ thin films*, Chalcogenide Letters, Vol. 10, No. 2, (2013), pp. 63-71

[57] Wee C. T., *Optical properties of amorphous selenium films*, MSc. Thesis: University of Saskatchewan, Saskatoon, Canada S7N5A9, (2006), pp. 4-119

[58] Kumar A., Heera P., Barma P. B., and Sharma R., *Optical properties of Bi doped Se-Te thin film*, Journal of Ovonic Research, Vol. 8, No. 5, (2012), pp. 135-146

[59] Connell G. A. N., *Optical properties of amorphous semiconductors*, Springer Berlin Heidelberg, Vol. 36, (1985), pp. 73-111

[60] Goswami, A., *Thin film fundamentals*, New Age International Publishers, New Delhi, India, (1997), pp. 419-450

[61] Tauc J., *Amorphous and Liquid Semiconductors*, Plenum Press, London and New York, (1974), pp. 171-194

[62] Ambika and Barman P. B., *Effect of Bi addition on the optical band gap of $Se_{85}Te_{15}$ Chalcogenide thin films*, Journal of Non-Oxide Glasses, Vol. 3, No. 2, (2012), pp. 19-24

[63] Mainika, Sharma P., Katyal S. C., and Thakur N., *A study of Impurities (Ag, Bi & Ge) on the optical properties of $Se - Te$ thin films*, Journal of Non-Oxide Glasses, Vol.1, No. 2, (2009), pp. 90-95

[64] Schottmiller J., Tabak M., Lucovsky G., and Ward A., *The effect of valency on transport properties of in vitreous binary alloys of selenium*, Journal of Non-Crystalline Solids, Vol. 4, (1970), pp. 80-96

[65] Hafiz M. M., Othmana A. A., El-Nahassb M. M., and Al-Motasema A. T., *Composition and thermal-induced effects on the optical constants of $Ge_{20}Se_{80-x}Bi_x$ thin films*, Physica B, Vol. 390, No. 1-2, (2007), pp. 348-355

[66] Bicerano J. and Ovshinsky S. R., *Chemical band approach to the structures of chalcogenide glasses with reversible switching properties*, Journal of Non-Crystalline Solids, Vol. 74, No.1, (1985), pp. 75-84